JOURNAL OF PETROLOGY | VOLUME 55 | NUMBER 11 | PAGES 2193–2216 | 2014 | doi:10.1093/petrology/egu054

Origin of the 'Ghost Plagioclase' Signature in Galapagos Melt Inclusions: New Evidence from Pb Isotopes

M. E. PETERSON[1]*, A. E. SAAL[1], E. NAKAMURA[2], H. KITAGAWA[2], M. D. KURZ[3] AND A. M. KOLESZAR[4]

[1]DEPARTMENT OF EARTH, ENVIRONMENTAL AND PLANETARY SCIENCES, BROWN UNIVERSITY, PROVIDENCE, RI 02912, USA

[2]THE PHEASANT MEMORIAL LABORATORY FOR GEOCHEMISTRY & COSMOCHEMISTRY, INSTITUTE FOR STUDY OF THE EARTH'S INTERIOR, OKAYAMA UNIVERSITY, MISASA, 682-0193, JAPAN

[3]DEPARTMENT OF MARINE CHEMISTRY AND GEOCHEMISTRY, WOODS HOLE OCEANOGRAPHIC INSTITUTION, WOODS HOLE, MA 02543, USA

[4]DEPARTMENT OF GEOLOGICAL SCIENCES, UNIVERSITY OF TEXAS AT AUSTIN, AUSTIN, TX 78712, USA

RECEIVED AUGUST 5, 2013; ACCEPTED SEPTEMBER 15, 2014
ADVANCE ACCESS PUBLICATION OCTOBER 22, 2014

Olivine-hosted melt inclusions from both Fernandina and Santiago islands in the Galapagos Archipelago have compositions indicating that plagioclase played an important role in the magmatic evolution of these volcanic islands. The major and trace element chemistry of the Santiago melt inclusions indicates simple plagioclase assimilation. In contrast, Fernandina inclusions have compositions for which the plagioclase appears to be present only as a 'ghost' trace element signature (i.e. 'ghost plagioclase' signature). Two competing hypotheses have been proposed to explain this unique signature: (1) incorporation of an ancient recycled plagioclase-rich cumulate into the mantle; (2) shallow-level interaction between melts and plagioclase-rich cumulates in the present-day lower oceanic crust. Here we present new Pb isotope measurements for olivine-hosted melt inclusions from Fernandina and Santiago islands to distinguish between the two models. The new Pb isotope data are within the range previously reported for whole-rock basalts from those islands. Melting and mixing models involving ancient (~0·5–1 Ga) recycled plagioclase-rich cumulates cannot reproduce the observed trace element and Pb isotopic characteristics of the Fernandina melt inclusions with a ghost plagioclase signature. Shallow-level diffusive interactions between basalt and present-day plagioclase-rich cumulates provide the simplest explanation for the observed trace element compositions and Pb isotope ratios of melt inclusions from Fernandina and Santiago islands.

KEY WORDS: *Galapagos; ghost plagioclase; mantle plume; melt inclusion; Pb isotopes*

INTRODUCTION

The magmatism of the Galapagos Archipelago (Fig. 1) has conventionally been described in terms of four end-member components based on Sr, Nd, Pb, Hf and noble gas (He, Ne) isotope data (Vicenzi *et al.*, 1990; Bow & Geist, 1992; White *et al.*, 1993; Reynolds & Geist, 1995; Kurz & Geist, 1999; Blichert-Toft & White, 2001; Harpp & White, 2001; Geist *et al.*, 2002; Saal *et al.*, 2007; Kurz *et al.*, 2009; Gibson *et al.*, 2012). The end-member compositions are expressed at individual islands, although several of these end-members are partially expressed at multiple volcanoes in the archipelago. Two enriched mantle components are best represented by lavas from Pinta and Floreana islands, a high $^{3}He/^{4}He$ component is characteristic of Fernandina lavas and a depleted component, similar to mid-ocean ridge basalt (MORB), is present in lavas from Genovesa Is. (Fig. 2). Previous geochemical studies of olivine-hosted melt inclusions and high-MgO basalts from the eastern central region of the Galapagos Archipelago indicate major and trace element and isotope

*Corresponding author. Telephone: +1 401 863 3339. Fax: +1 401 863-2058. E-mail address: mary.peterson@brown.edu

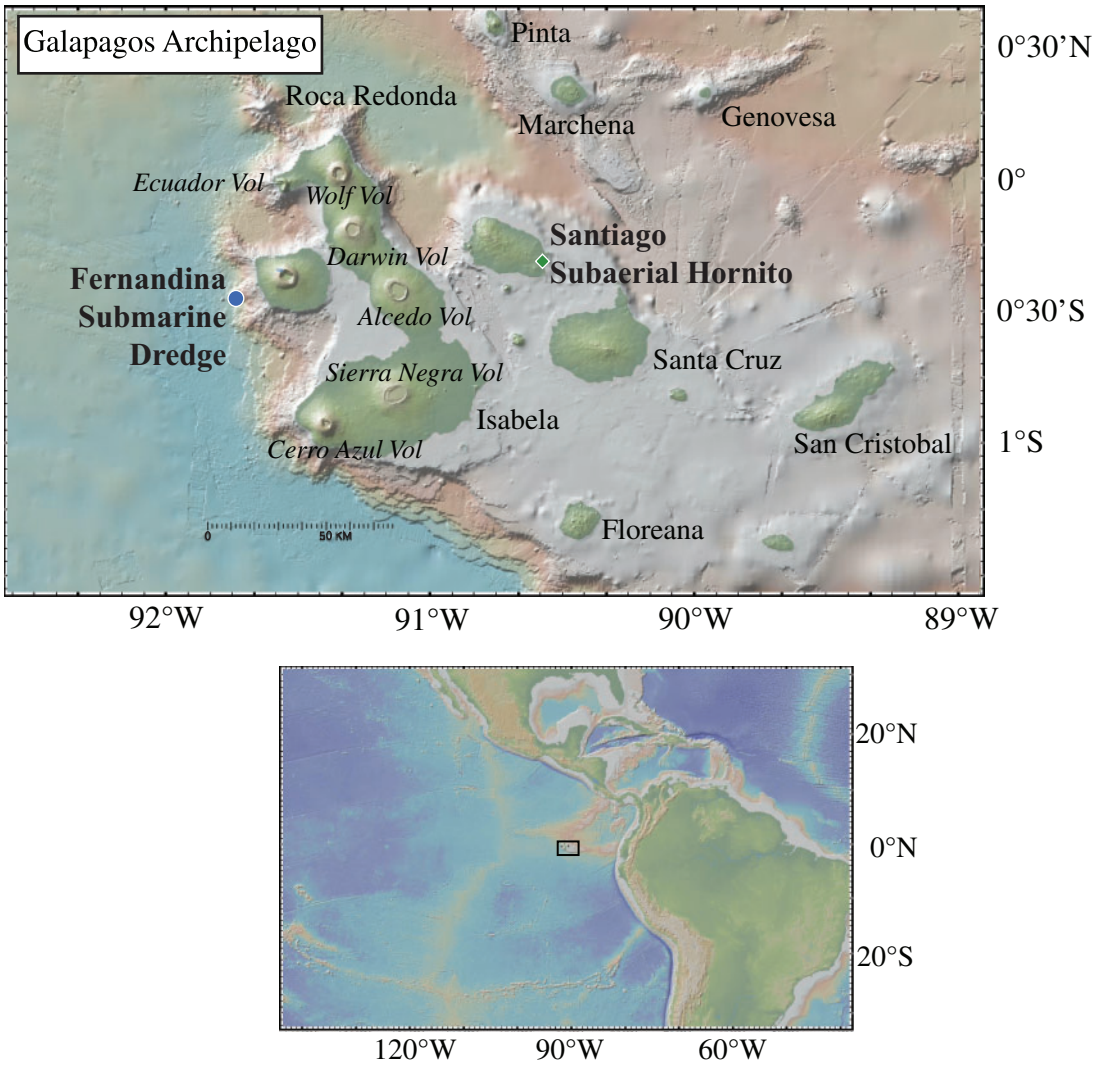

Fig. 1. Map indicating the locations of the submarine dredge from Fernandina Island and the subaerial hornito from Santiago Island from which the melt inclusions were analyzed.

signatures consistent with interaction between basalt and plagioclase-rich cumulates during melt percolation through the oceanic lithosphere (Saal *et al.*, 2007; Koleszar *et al.*, 2009). In contrast, geochemical data for Fernandina and Isabela Island basalts in the western part of the archipelago do not show evidence of plagioclase assimilation. However, some Fernandina melt inclusions do show strong trace element evidence of plagioclase assimilation, whereas the associated major element signature of this process is absent.

Detailed trace element studies of basalts and melt inclusions from several oceanic islands (including the Galapagos Archipelago) and mid-ocean ridges have shown the presence of an unusual composition characterized by Sr, Ba, and Eu anomalies greater than unity on primitive mantle normalized diagrams (Gurenko & Chaussidon, 1995; Hofmann & Jochum, 1996; Kamenetsky *et al.*, 1998; Yang *et al.*, 1998; Chauvel & Hemond, 2000; Sobolev *et al.*, 2000; Kent *et al.*, 2002; Danyushevsky *et al.*, 2003; Huang *et al.*, 2005; Ren *et al.*, 2005; Maclennan, 2008). Melting or crystallization will not significantly fractionate these elements from elements of comparable incompatibility unless plagioclase is involved. However, although the observed geochemical signature is typical of plagioclase-rich cumulates, many of these lavas and associated olivine-hosted melt inclusions show no indication of plagioclase accumulation or assimilation in their major element compositions (e.g. uncommon enrichment of Al_2O_3 and depletion of FeO with decreasing MgO content). Consequently, this unusual composition has been named the 'ghost plagioclase' signature (Sobolev *et al.*, 2000).

Most lavas and melt inclusions with a ghost plagioclase signature are characterized by very primitive compositions

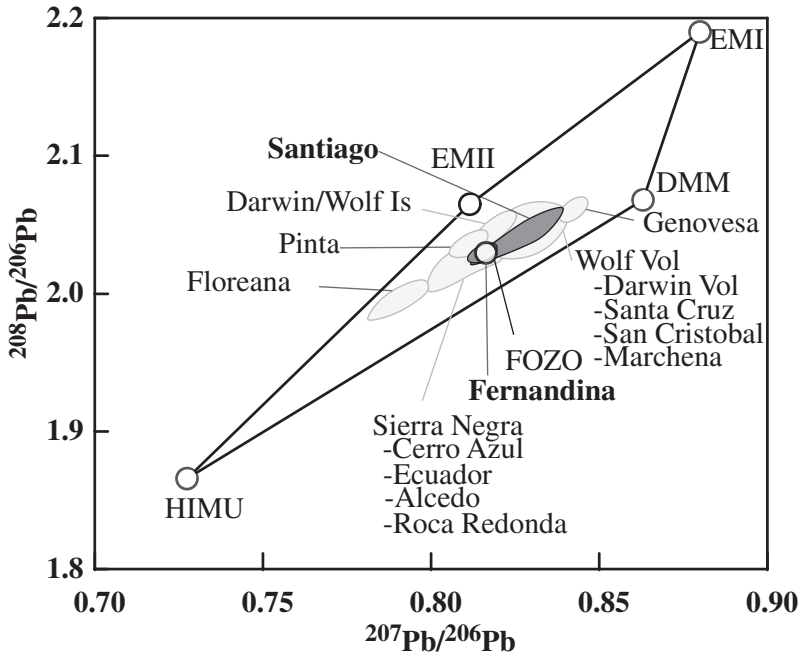

Fig. 2. $^{208}Pb/^{206}Pb$ vs $^{207}Pb/^{206}Pb$ obtained by thermal ionization mass spectrometry and multicollector inductively coupled plasma mass spectrometry for whole-rock and glass samples from the Galapagos archipelago. The data used are from Vicenzi *et al.* (1990), Bow & Geist (1992), White *et al.* (1993), Reynolds & Geist (1995), Harpp & White (2001), Geist *et al.* (2002) and Saal *et al.* (2007). Large open circles represent the four end-members of the mantle tetrahedron projected onto the $^{208}Pb/^{206}Pb$–$^{207}Pb/^{206}Pb$ plane (Hart, 1988; Hart *et al.*, 1992; Workman *et al.*, 2004; Stracke *et al.*, 2005). FOZO is the approximate position of the highest $^{3}He/^{4}He$ samples from the Galapagos in Pb isotope space. Light grey fields represent single Galapagos volcanoes; dark grey fields represent the data for Santiago and Fernandina islands.

(e.g. high MgO contents). This suggests that a plagioclase-rich component is required either in the melt source region or in the crust through which the melt percolates. Two main hypotheses have been proposed to explain this signature. The first considers the presence of ancient recycled oceanic crust containing plagioclase-rich cumulate gabbro (now eclogite) as a component intrinsic to the convecting mantle (Hofmann & Jochum, 1996; Chauvel & Hemond, 2000; Sobolev *et al.*, 2000; Kent *et al.*, 2002; Ren *et al.*, 2005). The second argues for the interaction of melts with plagioclase-rich cumulates during melt percolation through the present-day oceanic lithosphere (Danyushevsky *et al.*, 2003, 2004; Saal *et al.*, 2007; Maclennan, 2008). The trace element contents of a 500 m gabbroic section of the oceanic crust drilled at Ocean Drilling Program (ODP) site 735, Leg 118, show a clear plagioclase-rich cumulate signature (Hart *et al.*, 1999). If this composition represents the lower oceanic crust, then both hypotheses may provide a reasonable explanation for the ghost plagioclase signature observed in oceanic basalts.

Pb isotopes provide an effective tool for determining which model best explains the ghost plagioclase signature. Basalts generated from a source containing an ancient (~0·5–1 Ga) recycled plagioclase-rich cumulate gabbro (now eclogite) will have much higher $^{207}Pb/^{206}Pb$ and $^{208}Pb/^{206}Pb$ than present-day end-member MORB. This is due to the lower (U, Th)/Pb ratio of a plagioclase-rich cumulate [0·05 U/Pb and 0·114 Th/Pb based on the average 'protolith' of Hart *et al.* (1999)] compared with that of the Earth's depleted upper mantle [0·18 U/Pb and 0·439 Th/Pb based on the depleted MORB mantle (DMM) composition of Workman & Hart (2005)]. In contrast, basaltic magmas percolating through the present-day oceanic lithosphere will attain, at most, similar $^{207}Pb/^{206}Pb$ and $^{208}Pb/^{206}Pb$ ratios to those of the plagioclase cumulates with which they interact.

In this study we present new Pb isotope data from geochemically well-characterized olivine-hosted melt inclusions from Santiago and Fernandina islands (representing the central–eastern and western regions of the Galapagos Archipelago, respectively) to test the origin of their ghost plagioclase trace element signature. These Pb isotope data are consistent with the interaction between rising melts and present-day plagioclase-rich cumulates in the oceanic lithosphere.

SAMPLE SELECTION AND PREVIOUS WORK

Our study focuses on olivine-hosted melt inclusions from two basalt samples from Fernandina and Santiago islands (Fig. 1). The Fernandina sample is AHA D25C, dredged from the western submarine flank of Fernandina (00°27·2'S, 91°44·6'W, average 2750 m depth) during the

AHA-NEMO2 cruise in 2000. This dredge is part of the normal series lavas described by Geist *et al.* (2006), with a composition similar to the aphyric subaerial lavas erupted in Fernandina (Allan & Simkin, 2000). Both the subaerial and submarine lavas of Fernandina are noted for their compositional homogeneity, which is thought to be the result of mixing in a common magma chamber within the crust below Fernandina (Allan & Simkin, 2000; Geist *et al.*, 2006). The Santiago sample, STG06-29, was collected from a subaerial hornito (0°19'5·2"S, 90°35'1·7"W) on the eastern side of Santiago; this is characterized by a MORB-like depleted signature (Baitis & Swanson, 1976; White *et al.*, 1993; Koleszar *et al.*, 2009; Gibson *et al.*, 2012).

Olivine-hosted melt inclusions were hand picked from the crushed basalts under a binocular microscope, mounted in indium metal, exposed and then polished down to 0·25 μm using diamond paste (Fig. 3). The melt inclusions are naturally quenched to a homogeneous glass and have shapes that indicate a primary origin (Sobolev, 1996). They range in size from 50 to 250 μm in diameter, with the inclusions from Santiago being, on average, smaller (~60 μm) than those from Fernandina (~125 μm).

Major and trace element compositions

The major and selected trace element contents of the melt inclusions, matrix glass and olivine host were reported by Koleszar *et al.* (2009). Complementary trace element data are reported here. The trace element data corrected for host olivine crystallization are included in Supplementary Data Electronic Appendix S1 (supplementary data are available for downloading at http://www.petrology.oxfordjournals.org). Analytical errors (2σ) for triplicate analyses of representative melt inclusions are <3% for SiO_2, CaO and Al_2O_3, <5% for MgO, TiO_2 and FeO, and <9% for Na_2O. For the olivine hosts the error is <2% for SiO_2, MgO and FeO. Errors for the trace elements, determined from replicate analyses of matrix glasses and large melt inclusions, are typically <5% (2σ). Major and trace elements were corrected for olivine crystallization on the interior wall of the inclusion by numerically adding host olivine back into the melt inclusion composition in 0·1% increments until the inclusion and olivine host are in MgO–FeO equilibrium. Samples required only 2·6–16 %, averaging 7·0% olivine addition. Further information on the analytical techniques and corrections has been given by Koleszar *et al.* (2009).

Olivine phenocrysts hosting the melt inclusions have Mg# [molar, 100MgO/(MgO + FeO)] averaging 85 ± 2 in the Fernandina sample and 86·6 ± 0·8, with only two exceptions having Mg# of 82 and 85, in the Santiago sample (Koleszar *et al.*, 2009). In both samples, the Mg# of the olivine in equilibrium with the matrix glass is 78 and 82 for Fernandina and Santiago olivines, respectively, indicating FeO–MgO disequilibrium between the phenocrysts and the host glasses.

The role of plagioclase: evidence from major and trace elements

Santiago inclusions

After correction for olivine crystallization, both the major and trace element compositions of the Santiago melt inclusions provide evidence for direct assimilation of plagioclase. Assimilation can be identified by a large decrease in FeO* (FeO* indicating total Fe) and a large increase in Al_2O_3 with decreasing MgO content, trends that cannot be reproduced by crystal fractionation processes (Fig. 4) (Koleszar *et al.*, 2009). Furthermore, almost all inclusions exhibit positive Sr, Ba, and Eu anomalies in primitive mantle normalized trace element patterns (Fig. 5) (Koleszar *et al.*, 2009). The magnitude of these anomalies correlates with Al_2O_3 contents; however, they do not show a correlation with highly incompatible trace element ratios (i.e., indicators of mantle enrichment). This suggests a common mantle source for the inclusions and assimilated plagioclase. (Fig. 6). If the variation in Al_2O_3 were the result of a different process from simple plagioclase assimilation (e.g. variable degrees of melting), we would expect a large range in trace element ratios of highly to moderately incompatible elements (e.g. La/Yb) associated with the Al_2O_3 variations. For most of the Santiago melt inclusions such a correlation is not observed (Koleszar *et al.*, 2009). Inclusion STG06-29-19 represents an extreme case, with the lowest incompatible trace element contents and the strongest Sr and Eu anomalies. Only one Santiago inclusion (STG06-29-10, labeled Santiago enriched composition in Fig. 4 and subsequent figures) has low Al_2O_3 and high FeO contents at low MgO coupled with a Sr anomaly lower than unity, indicating possible plagioclase fractionation prior to entrapment.

Fernandina inclusions

Although the major element compositions of the Fernandina melt inclusions indicate fractional crystallization, the trace element compositions of a subgroup of inclusions indicate a ghost plagioclase signature. The major element contents of the inclusions, when combined with a compilation of Fernandina submarine glasses (Geist *et al.*, 2006), can be simply explained by a sequence of olivine, olivine–plagioclase and olivine–plagioclase–clinopyroxene crystallization (Fig. 4). However, the trace element contents of the inclusions define two distinct groups: one with an enriched incompatible trace element composition typical of Fernandina lavas and a second group with an incompatible trace element depleted composition. Eight of the 11 inclusions with depleted trace element compositions have positive Sr, Ba, and Eu anomalies in a primitive mantle normalized diagram (Figs 5 and 6), but their major element contents are inconsistent with the assimilation of plagioclase (i.e. ghost plagioclase signature). The magnitudes of the Sr, Ba, and Eu anomalies do not correlate with Al_2O_3 content (Fig. 6). However, a weak

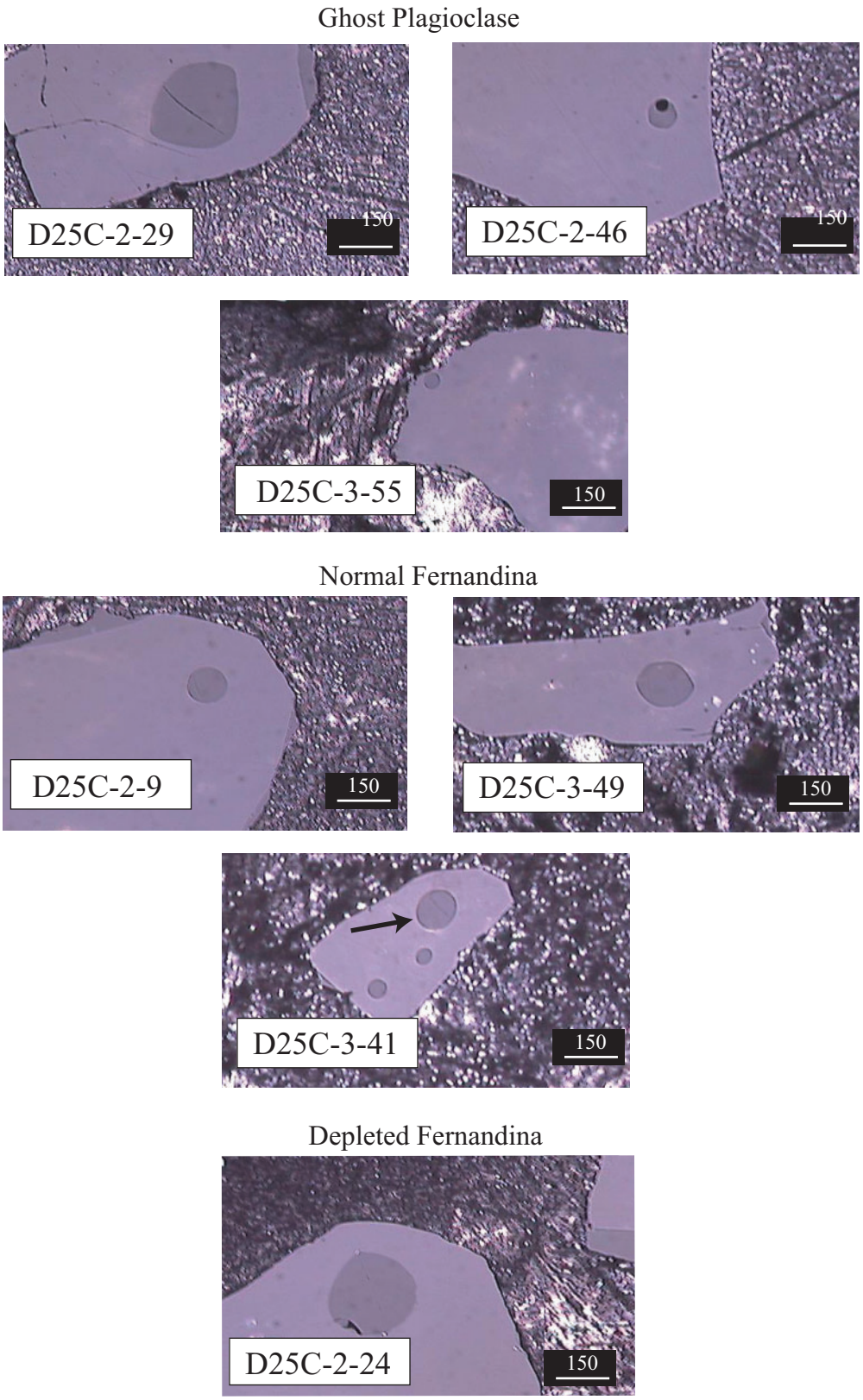

Fig. 3. Photomicrographs of representative olivine-hosted melt inclusions from Fernandina and Santiago basalts taken in reflected light. In olivine grains with multiple exposed inclusions, a black arrow indicates the inclusion that was analyzed. There is no significant difference in appearance between the Fernandina melt inclusions with the ghost plagioclase signature, the depleted, and the normal inclusions (similar to the matrix glass). This is also true for the Santiago normal, enriched, and depleted inclusions. Scale bar units are in μm.

(continued)

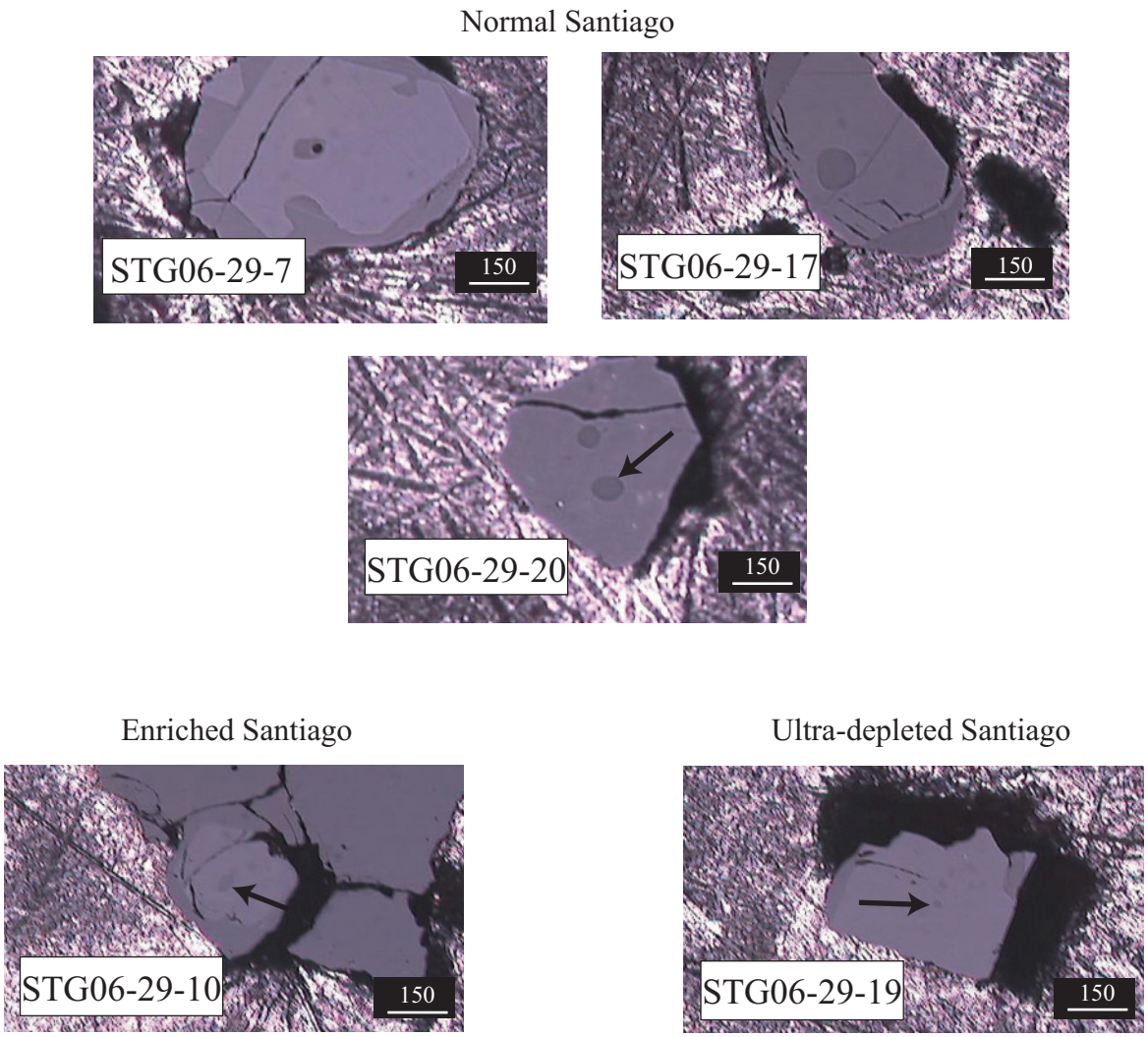

Fig. 3. Continued.

negative correlation exists between Sr/Sr* $\{Sr_{PM}/[(Ce_{PM}+Nd_{PM})/2]\}$ and Nb/La, which indicates the involvement of a trace element depleted melt in the creation of the ghost plagioclase signature.

ANALYTICAL METHODS FOR Pb ISOTOPES

Pb isotope analyses (Table 1) were performed by secondary ion mass spectrometry (SIMS) using the Cameca 1270 system at the Institute for the Study of the Earth's Interior, Okayama University, Misasa, Japan. In preparation for using the ion probe, mounts were submerged in 0·5M HNO_3 for 5 min to remove any sources of contamination from the surface. The samples were rinsed with MilliQ water three times, left under vacuum overnight to dry and coated with 300 Å of gold.

The samples were sputtered using a 30 nA focused beam of O^- ions resulting in a 30 μm diameter pit. The primary beam (acceleration) energy was 23 keV, and the secondary accelerating voltage was 10 keV. Samples were analyzed at a mass resolution of 3000. Pb isotopes were collected using a multi-collection system equipped with five electron multipliers following the methods described by Kobayashi *et al.* (2004). Each analysis consisted of 3 min of pre-sputtering followed by 400 cycles of 10 s on Pb peaks. Mass positions were set by centering the ^{206}Pb peak at the beginning of each analysis owing to the high concentration of Pb in the standard. Background runs were measured using the settings of the run, but without the primary beam emission, and routinely checked throughout the session.

We used the synthetic basaltic glass standard FMSA (5 ppm Pb) to correct for instrumental mass

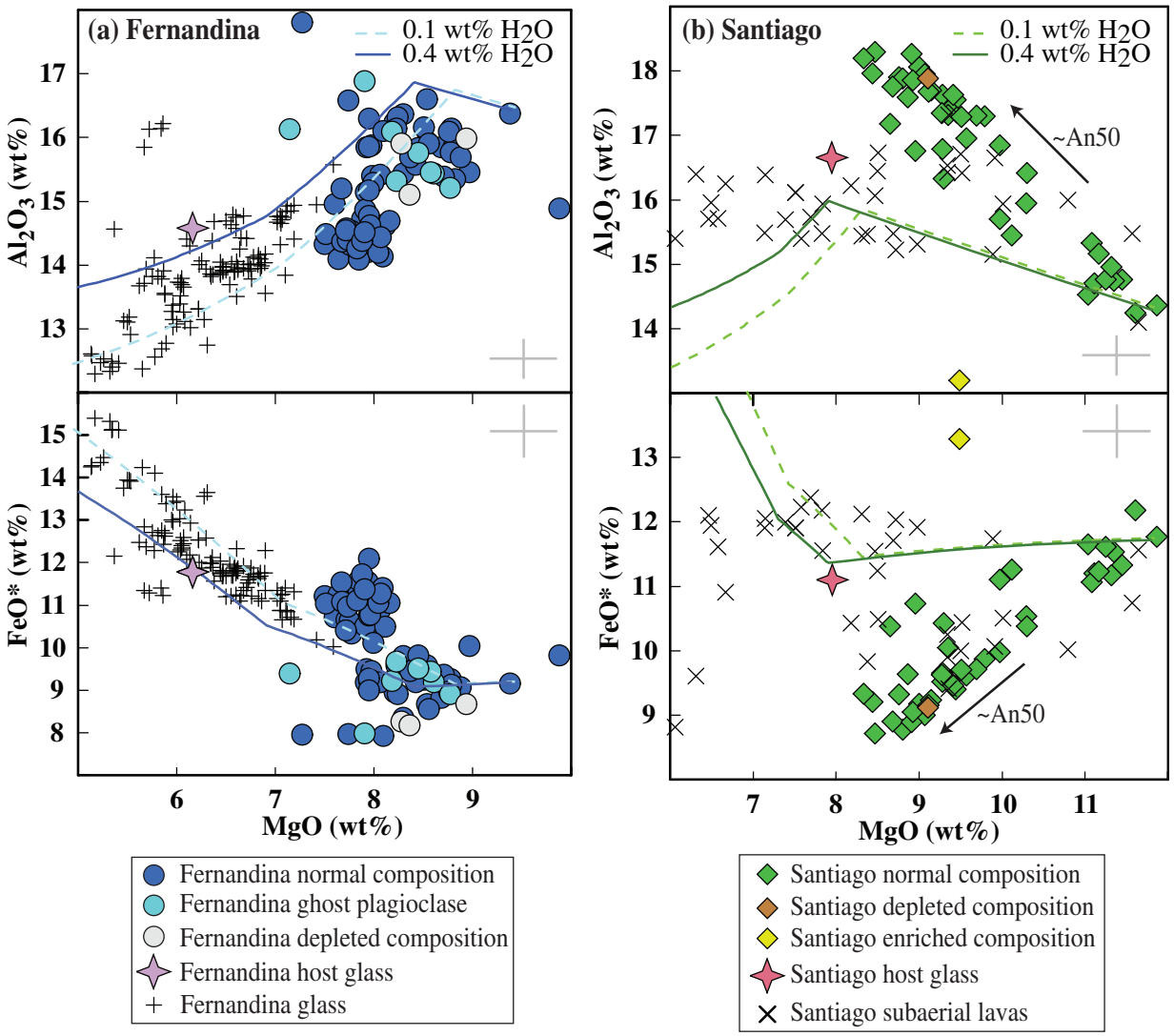

Fig. 4. Variation of Al_2O_3 and FeO* (total iron reported as FeO) vs MgO wt %. (a) Fernandina melt inclusions (Koleszar *et al.*, 2009) and compiled glass data (Geist *et al.*, 2006). Dark blue circles, melt inclusions with trace element compositions similar to the Fernandina host glass (Fernandina normal composition); light grey circles, depleted trace element compositions; cyan circles, melt inclusions with ghost plagioclase signature; violet star, Fernandina host glass composition. (b) Santiago melt inclusions (Koleszar *et al.*, 2009) and a compilation of Santiago subaerial lavas (data from http://georoc.mpch-mainz.gwdg.de/georoc). Dark green diamonds, melt inclusions with trace element composition similar to Santiago host glass (Santiago normal composition); yellow diamond, enriched trace element composition (STG06-29-10); brown diamond, extreme trace element depletion and plagioclase signature (STG06-29-19); pink star, Santiago host glass composition. Average 2σ error shown by the grey cross. Crystal fractionation trends were calculated using PETROLOG (Danyushevsky, 2001; Danyushevsky & Plechov, 2011) for both Santiago and Fernandina melt inclusions at a pressure of 1·5 kbar for two concentrations of water: dashed line, 0·1 wt %; continuous line, 0·4 wt % water. Starting melt compositions for the calculations were chosen to be the high MgO content inclusions D25C-3-20 and STG06-29-06 for Fernandina and Santiago, respectively. It should be noted that, in general, the Fernandina inclusions define a trend that can be produced by magmatic differentiation of olivine, followed by olivine + plagioclase, followed by olivine + plagioclase + clinopyroxene. The inclusions with the ghost plagioclase signature also fall along this trend at major element concentrations indistinguishable from the normal Fernandina inclusions. In contrast, Santiago inclusions cannot be reproduced by simple magmatic differentiation; their increase in Al_2O_3 and decrease in FeO* with decreasing MgO wt % cannot be reproduced by normal crystal fractionation and represent the assimilation of plagioclase of approximately An_{50}.

discrimination (Kobayashi *et al.*, 2004). The standard was measured repeatedly (≥9 times per day) over the course of the session. The daily external precision for the standard (2σ standard deviation of daily group of standard measurements) ranges from ±0·27% ($n=16$) to 0·35% ($n=9$) for $^{207}Pb/^{206}Pb$ and 0·24% ($n=9$) to 0·35% ($n=16$) for $^{208}Pb/^{206}Pb$.

The Pb concentrations of the melt inclusions are all <2 ppm, leading to low precision in the measured isotopic ratios. In the case of the Santiago inclusions, with Pb

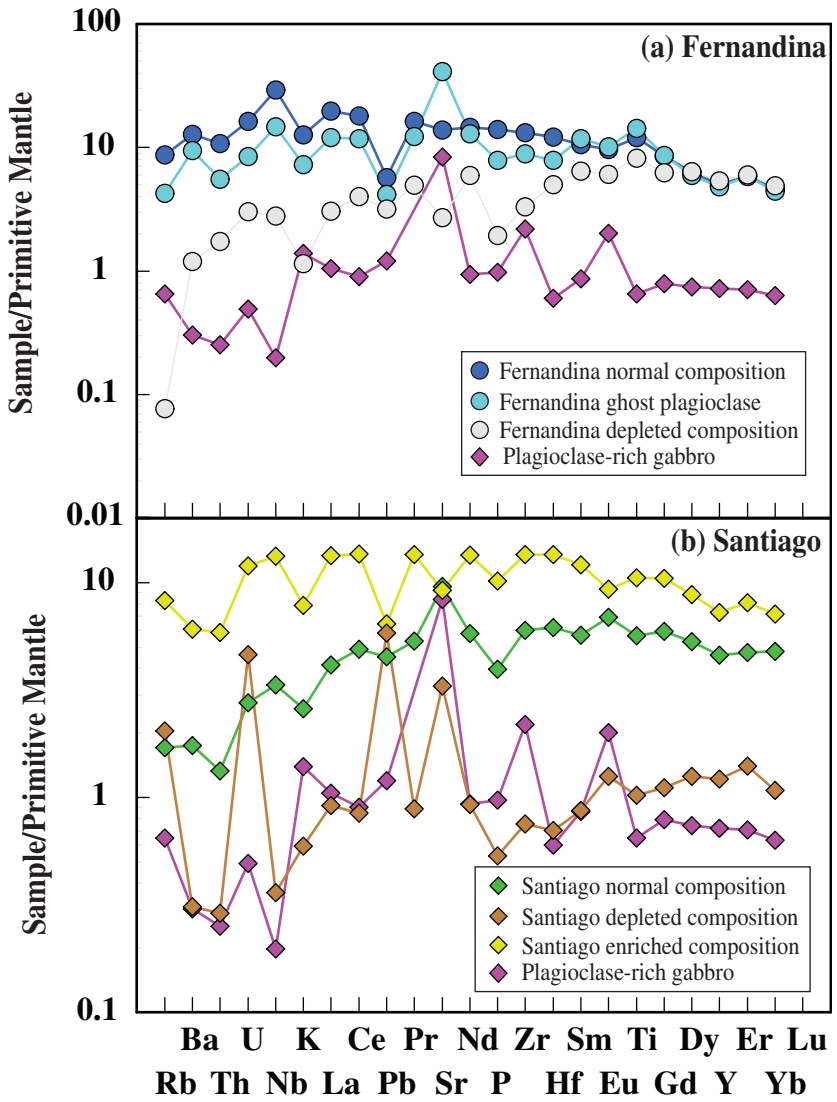

Fig. 5. Primitive mantle-normalized trace element patterns for representative samples. (a) Fernandina: normal composition melt inclusion D25C-3-12 (MgO wt % = 8·51), depleted trace element composition D25C-2-24 (MgO wt % = 8·34), and ghost plagioclase composition D25C-3-34 (MgO wt % = 8·58). (b) Santiago: normal composition melt inclusion STG-06-29-17 (MgO wt % = 9·79), enriched composition STG06-29-10 (MgO wt % = 9·47), and most depleted trace element composition STG06-29-19 (MgO wt % = 9·10). Normalizing values are from McDonough & Sun (1995). Also plotted in (a) and (b) is the lower crustal plagioclase-rich gabbro protolith (Hp) reported by Hart *et al.* (1999).

concentrations of 0·6–0·9 ppm, the 2σ standard error in Pb isotope ratio is in the range of ±0·6–1·5% for $^{207}Pb/^{206}Pb$ and ±0·5–1·1% for $^{208}Pb/^{206}Pb$. For the Fernandina inclusions, with Pb concentrations of 0·5–1·5 ppm, the errors are ±0·4–2% and ±0·3–1·6% for $^{207}Pb/^{206}Pb$ and $^{208}Pb/^{206}Pb$, respectively. The low ^{204}Pb ion current yielded large uncertainties in the ^{204}Pb-normalized isotope ratios, rendering these ratios unusable.

RESULTS

The Pb isotopic compositions of the melt inclusions are consistent with those previously reported for whole-rock samples from Fernandina and Santiago islands (White *et al.*, 1993; Harpp & White, 2001; Saal *et al.*, 2007; Gibson *et al.*, 2012; Fig. 7).

For Santiago inclusions, $^{207}Pb/^{206}Pb$ ranges from 0·8261 to 0·8473, and $^{208}Pb/^{206}Pb$ from 2·0335 to 2·0678, which is within error of the range reported for Santiago whole-rock samples ($^{207}Pb/^{206}Pb = 0·8133–0·8381$ and $^{208}Pb/^{206}Pb = 2·0237–2·0569$) (White *et al.*, 1993; Saal *et al.*, 2007; Gibson *et al.*, 2012). There is no significant correlation between Pb isotope ratios and the major and trace element contents indicative of plagioclase assimilation typical of these inclusions (Fig. 8). Inclusion

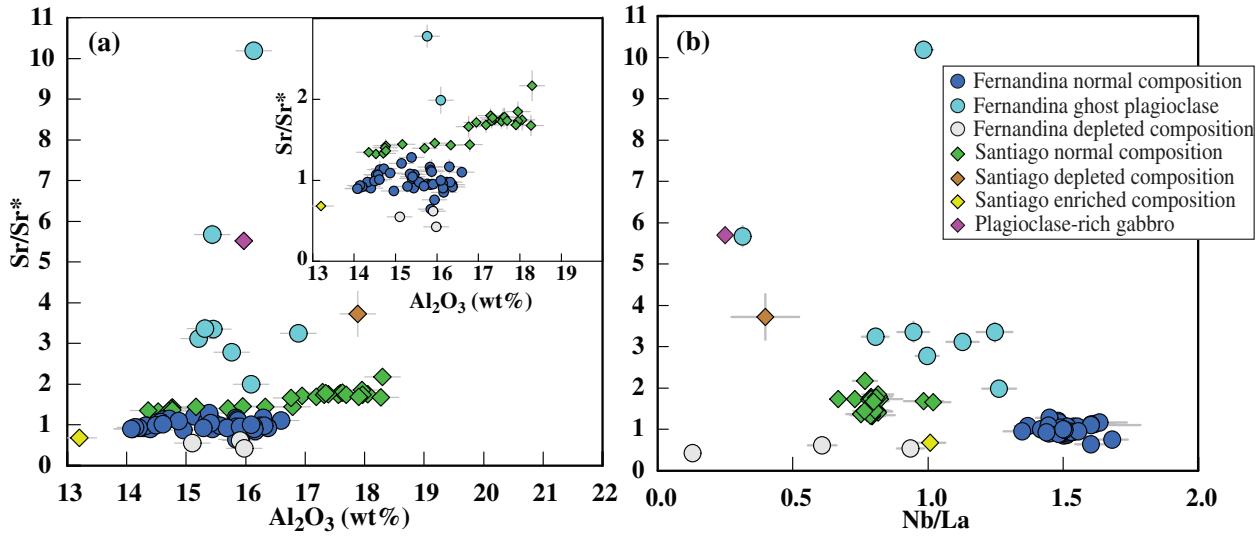

Fig. 6. (a) Sr/Sr* $\{Sr_{PM}/[(Ce_{PM}+Nd_{PM})/2]\}$ vs Al_2O_3 wt % for single melt inclusions from Fernandina and Santiago islands. The inset shows a close-up view to better illustrate the correlation between Sr/Sr* and Al_2O_3 in the Santiago inclusions. (b) Sr/Sr* vs Nb/La for Fernandina and Santiago inclusions. The plagioclase-rich gabbro sample plotted is the protolith gabbro sample Hp (Hart *et al.*, 1999).

STG06-29-10 (Santiago enriched inclusion, which exhibits major and trace element evidence for plagioclase fractionation) has Pb isotope ratios within the range of the typical Santiago inclusions. STG06-29-19 (highest Sr anomaly) was too small in size to obtain reliable Pb isotope data.

In the Fernandina inclusions, $^{207}Pb/^{206}Pb$ ranges from 0·8113 to 0·8240 and $^{208}Pb/^{206}Pb$ from 2·010 to 2·042, which is within error of the range for Fernandina whole-rock isotopic data reported in the literature ($^{207}Pb/^{206}Pb = 0·8136–0·8168$ and $^{208}Pb/^{206}Pb = 2·0281–2·0316$) (White *et al.*, 1993; Kurz & Geist, 1999; Saal *et al.*, 2007). The average of the melt inclusion range ($^{207}Pb/^{206}Pb = 0·8174$, $^{208}Pb/^{206}Pb = 2·0315$, weighted for Pb concentration) falls close to the value of the host lava AHA D25C (Fig. 7). This is consistent with the host lava being a heterogeneous mixture of melts with varied geochemical compositions that the melt inclusions are sampling more fully (Saal *et al.*, 2005; Maclennan, 2008). There is no discernible correlation between the Pb isotope, major, or trace element composition of the inclusions (Fig. 8). The inclusions with depleted incompatible trace element contents we were able to measure have, at similar $^{207}Pb/^{206}Pb$, unusually high $^{208}Pb/^{206}Pb$. However, the large errors in these two analyses, owing to the low Pb concentrations of the inclusions, do not allow us to discuss further the implications of these results. From the eight inclusions with ghost plagioclase signature only four were large enough to measure the Pb isotope composition. These four inclusions have $^{207}Pb/^{206}Pb$ and $^{208}Pb/^{206}Pb$ within the range of the other Fernandina inclusions.

DISCUSSION

Evidence for contamination by plagioclase cumulates: relationship between major elements, trace elements and Pb isotopes

Santiago melt inclusions (normal and enriched) have Pb isotope compositions that are within the range of those previously measured on whole-rock lavas from this island and indicate the presence of both trace element and Pb isotope enriched and depleted melt components (White *et al.*, 1993; Gibson *et al.*, 2012). Although the melt inclusions provide major and trace element evidence for the assimilation and crystal fractionation of plagioclase, their Pb isotope ratios do not significantly correlate with any chemical indicators of these processes. There is, if any, only a very weak positive trend between Pb isotope ratios and both Al_2O_3 content and Sr/Sr* (Fig. 8). This indicates that the inclusions with depleted trace element signatures and high $^{207}Pb/^{206}Pb$ and $^{208}Pb/^{206}Pb$ have been more affected by assimilation of plagioclase cumulates than the enriched inclusions, consistent with the hypothesis proposed by Saal *et al.* (2007) based on whole-rock geochemical data for basalts from the Galapagos Archipelago.

The assimilation of plagioclase is responsible for the observed range in Sr/Sr* and Nb/La seen in the normal Santiago inclusions (Fig. 6); this process changes the Sr/Sr* without significant modification of the Nb/La ratio in the melt. The exception is the depleted Santiago inclusion that has a Nb/La ratio much lower than the normal Santiago inclusions (0·4 compared with 0·8, respectively). This ratio cannot be explained by a normal Santiago melt

Table 1: Pb isotope compositions of Santiago and Fernandina melt inclusions and Fernandina host glass

Sample	$^{207}Pb/^{206}Pb$	2σ	$^{208}Pb/^{206}Pb$	2σ
Santiago				
STG06-29-02A	0·8262	0·0090	2·052	0·019
STG06-29-02B	0·8343	0·0067	2·035	0·014
STG06-29-03	0·8405	0·0065	2·051	0·013
STG06-29-7	0·8473	0·0063	2·065	0·013
STG06-29-13	0·8268	0·0065	2·034	0·013
STG06-29-16B	0·8406	0·0124	2·068	0·024
STG06-29-16C	0·8335	0·0068	2·064	0·015
STG06-29-17	0·8389	0·0062	2·058	0·012
STG06-29-20	0·8353	0·0078	2·045	0·016
STG06-29-24	0·8324	0·0077	2·046	0·015
STG06-29-25	0·8261	0·0068	2·048	0·015
STG06-29-47	0·8332	0·0072	2·054	0·014
Santiago enriched				
STG06-29-10	0·8298	0·0052	2·049	0·010
Fernandina normal				
D25C-2-9	0·8194	0·0034	2·032	0·007
D25C-2-19A	0·8169	0·0038	2·027	0·008
D25C-2-19B	0·8143	0·0058	2·010	0·012
D25C-2-25A	0·8150	0·0069	2·016	0·015
D25C-2-27	0·8177	0·0036	2·031	0·007
D25C-2-30	0·8164	0·0035	2·036	0·007
D25C-2-52A	0·8113	0·0044	2·031	0·009
D25C-2-54	0·8129	0·0036	2·020	0·007
D25C-2-55	0·8179	0·0053	2·034	0·011
D25C-2-59	0·8206	0·0040	2·034	0·008
D25C-2-62	0·8146	0·0037	2·031	0·008
D25C-3-07	0·8228	0·0043	2·042	0·009
D25C-3-10	0·8240	0·0041	2·037	0·008
D25C-3-12	0·8213	0·0039	2·038	0·008
D25C-3-14	0·8192	0·0034	2·041	0·007
D25C-3-31	0·8193	0·0038	2·030	0·008
D25C-3-41A	0·8168	0·0038	2·024	0·008
D25C-3-42	0·8127	0·0039	2·028	0·009
D25C-3-43	0·8209	0·0043	2·042	0·008
D25C-3-49	0·8166	0·0047	2·026	0·010
D25C-3-52	0·8143	0·0043	2·027	0·009
Fernandina ghost plagioclase				
D25C-2-29	0·8211	0·0086	2·028	0·017
D25C-2-46	0·8284	0·0169	2·040	0·033
D25C-3-34	0·8181	0·0076	2·032	0·016
D25C-3-55	0·8149	0·0067	2·037	0·015
Fernandina depleted				
D25C-2-24	0·8192	0·0135	2·050	0·028
D25C-2-57	0·8120	0·0153	2·052	0·034
Host glass				
AHA D25C glass	0·8155		2·031	

Pb isotopic ratios and error are 2σ standard error for Santiago melt inclusions and Fernandina melt inclusions. Fernandina inclusions were separated into normal, ghost plagioclase, and depleted based on the differing trace element signatures of the inclusions. The Santiago inclusion with the trace element enriched composition is also separated from the normal composition Santiago inclusions.

undergoing simple plagioclase assimilation and therefore requires the presence of a more depleted melt (with low Nb/La) within the magmatic plumbing system beneath Santiago. It is unfortunate that the depleted Santiago inclusion (STG06-29-19) was too small in size to obtain reliable Pb isotope data.

The Pb isotopic compositions of the Fernandina inclusions fall within error of the range defined by the lavas from this island. This is expected for inclusions with major and trace element compositions analogous to Fernandina whole-rock lavas. However, inclusions with a ghost plagioclase signature have Pb isotope compositions indistinguishable from those of normal Fernandina inclusions (Figs 7 and 8). This suggests that the process producing the ghost plagioclase signatures in the Fernandina inclusions does not significantly affect the Pb isotope ratios of the melt.

Evaluating the two theories for the origin of the Fernandina 'ghost plagioclase signature'

With the new Pb isotopic constraint it is possible to evaluate the two proposed models for the origin for the ghost plagioclase signature: ancient recycled oceanic crust versus interaction with present-day plagioclase-rich cumulates. Whereas the two models are indistinguishable with respect to major and trace element concentrations, their Pb isotopes will be significantly different. Here, we evaluate both models for their ability to reproduce the trace element and Pb isotopic signatures of the Fernandina inclusions.

Estimating the Pb isotope composition of ancient plagioclase cumulates

To estimate the Pb isotope ratios of an ancient (~0·5–1 Ga) recycled plagioclase cumulate we assume that the

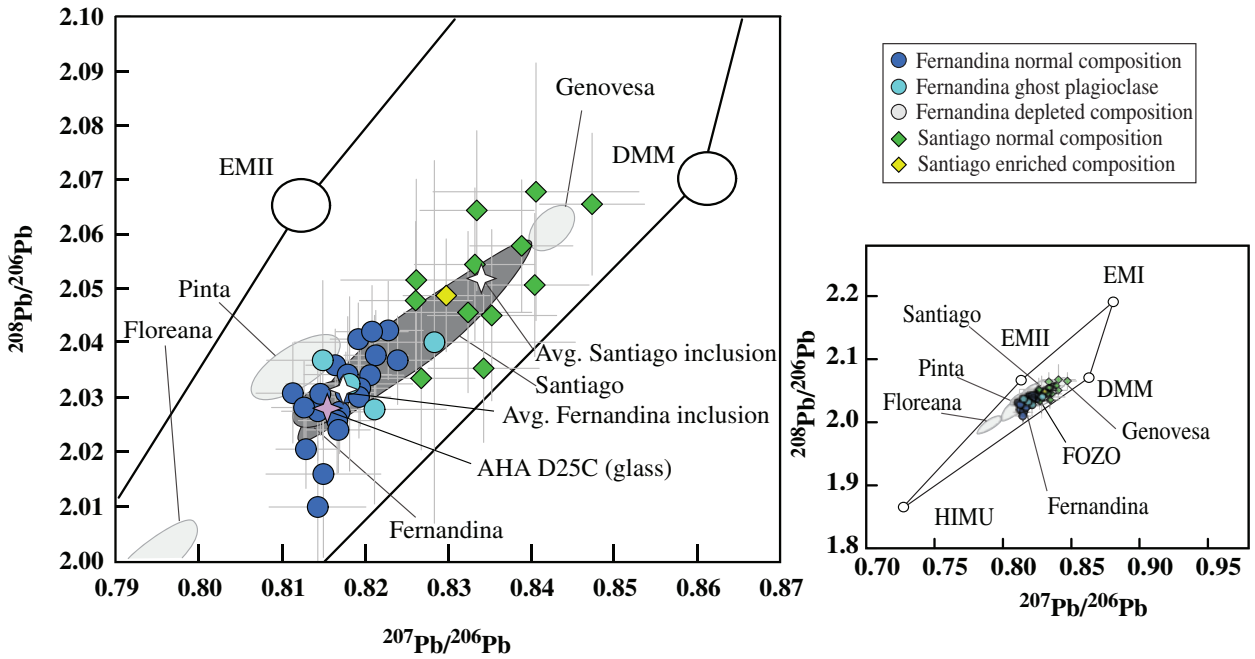

Fig. 7. $^{208}Pb/^{206}Pb$ vs $^{207}Pb/^{206}Pb$ ratios for single melt inclusions from both Santiago and Fernandina islands. The data are overlain on the fields for Fernandina and Santiago whole-rock lavas (data sources as in Fig. 2). Also plotted is the Fernandina host glass AHA D25C (violet star), and an average weighted for Pb concentration of the Fernandina melt inclusions and Santiago melt inclusions (white stars). The inset shows a smaller-scale view of the data. It should be noted that the inclusions with the ghost plagioclase signature plot in the same isotopic space as the inclusions from Fernandina with normal trace element compositions.

cumulate is formed in the oceanic lithosphere during the crystallization of a range of MORB compositions. Using the present-day Pb isotope composition of Pacific MORB and the U, Th and Pb contents estimated for MORB-source mantle [E-DMM, N-DMM and D-DMM (enriched, normal and depleted MORB mantle); Donnelly *et al.*, 2004; Stracke *et al.*, 2005; Workman & Hart, 2005], we calculate the Pb isotope composition of the plagioclase-rich cumulate at the time of its formation (~0·5–1 Ga). We then use these calculated Pb isotope ratios with the measured U, Th and Pb concentrations of plagioclase-rich cumulates in the oceanic crust (Zimmer *et al.*, 1995; Hart *et al.*, 1999) to calculate its present-day Pb isotopic composition. Present-day Pb isotope ratios of the ancient plagioclase cumulate calculated by this model are inconsistent with the values measured in Fernandina melt inclusions with ghost plagioclase signatures (Fig. 9).

The main variable parameters that control the isotopic evolution of the recycled gabbro in the calculation described above are the present-day isotopic and trace element composition of the MORB source, the trace element composition of the gabbro, and time. The boundaries of the isotopic composition of the MORB source are defined by a compilation of Pacific MORB isotope data ($^{207}Pb/^{206}Pb = 0·82–0·88$, $^{208}Pb/^{206}Pb = 2·026–2·120$; Stracke *et al.*, 2005). These boundaries contain E-, N- and D-MORB isotopic values. As such, we change the U, Th, and Pb contents with the isotopic values to reflect the difference in trace element enrichment of E-MORB versus N- and D-MORB sources (Donnelly *et al.*, 2004; Workman & Hart, 2005). For the trace element composition of the gabbro we use reported U, Th, and Pb contents measured for what are considered pristine, unaltered protoliths (i.e. Hp) and variably hydrothermally altered strip samples (i.e. Ps, Qs, Os) of lower crustal gabbros that show trace element evidence for plagioclase accumulation [reported by Hart *et al.* (1999)], and an average Gabbal Gerf plagioclase-rich gabbro composition (GG) as an additional composition to test (Zimmer *et al.*, 1995). Therefore both a range in U/Pb (0·018–0·176) and Th/Pb ratios (0·032–0·484) were input into the calculation. We test ages of 500 Ma and 1 Ga for the recycled gabbro. The 500 Ma minimum time of evolution is a conservative average minimum recycling time found through simultaneous analysis of multiple isotopic systems at other hotspots (e.g. McKenzie *et al.*, 2004), whereas material older than 1 Ga did not show significant result improvement. All parameters are listed in Table 2 and the results are shown in Fig. 9.

Although subduction may affect the U, Th, and Pb contents of plagioclase-rich cumulate gabbros, what precisely this effect is remains largely unconstrained. The study of Becker *et al.* (2000) approached this problem by studying high-pressure eclogite-bearing terranes. Those samples

Figure 8

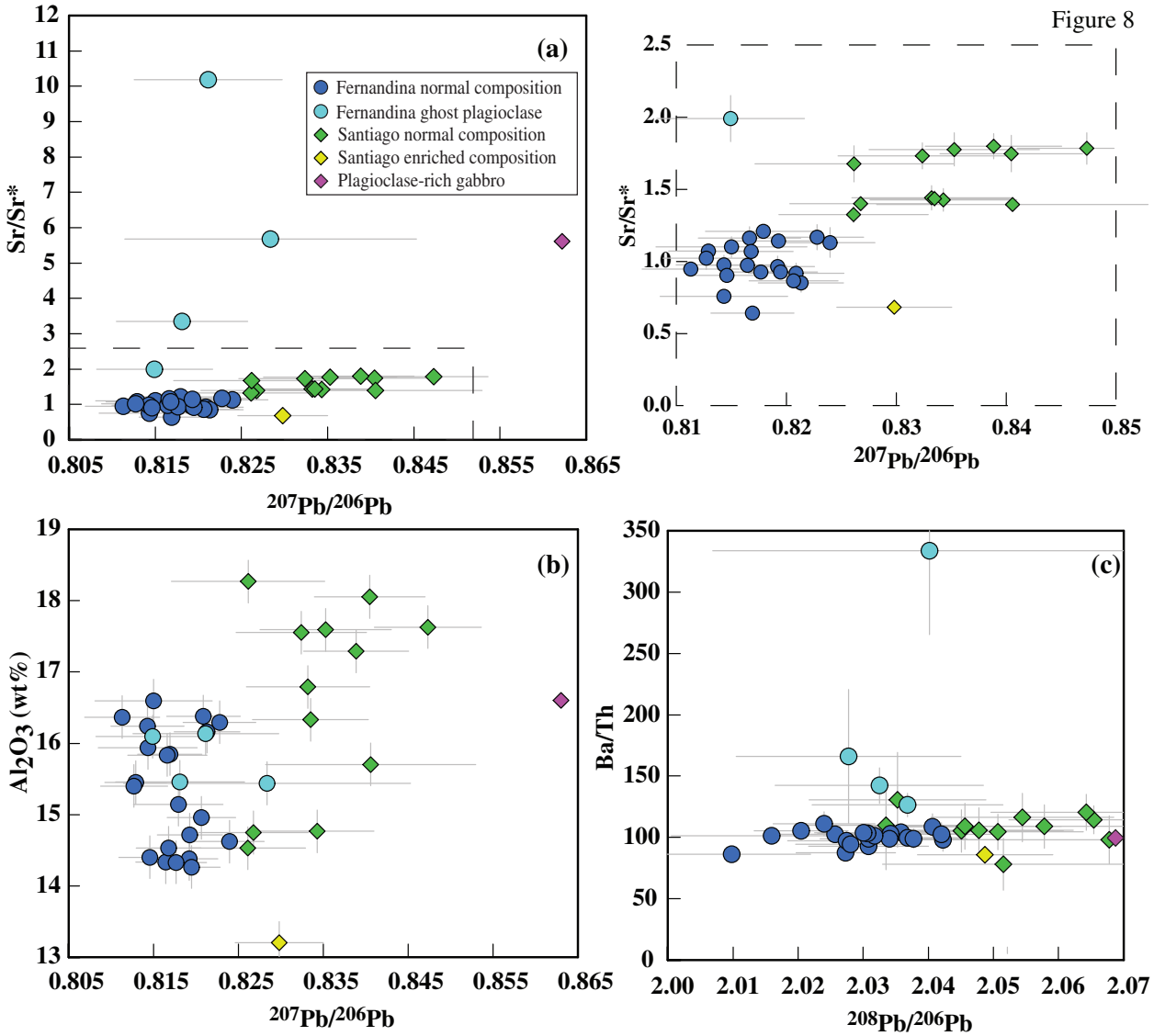

Fig. 8. (a) Sr/Sr* ($Sr_{PM}/[(Ce_{PM}+Nd_{PM})/2]$) vs $^{207}Pb/^{206}Pb$ ratios for Fernandina and Santiago melt inclusions. A close-up view of the data is shown to the right. It should be noted that Sr/Sr*, an indicator of a plagioclase signature, does not correlate with $^{207}Pb/^{206}Pb$ for either Fernandina or Santiago. (b) Al_2O_3 wt % vs $^{207}Pb/^{206}Pb$ for Fernandina and Santiago inclusions. It should be noted that a very weak correlation might exist only for the Santiago melt inclusions. (c) Ba/Th vs $^{208}Pb/^{206}Pb$ for Fernandina and Santiago melt inclusions. There is no clear correlation between Ba/Th and Pb isotopic ratio. Also plotted is the plagioclase-rich gabbro composition of protolith gabbro Hp from Hart *et al.* (1999) with the isotopic composition of average DMM (Stracke *et al.*, 2005).

with a gabbroic protolith were comparable with samples from the lower oceanic crust, which suggests that subduction does not have a significant affect on the U, Th, and Pb contents of subducted plagioclase cumulates. Other studies have tried to quantify the trace element flux in a subduction zone using mass-balance calculations (e.g. Kelley *et al.*, 2005; Chauvel *et al.*, 2009; Porter & White, 2009). Porter & White (2009), using data from eight subduction zones for their trace element flux calculation, found that, on average, 73–79% of the U, Th, and Pb survived into the deep mantle, making changes to U/Pb, Th/Pb and Th/U small and not systematic. Therefore, for our model we consider the U/Pb and Th/Pb ratios of the recycled plagioclase cumulate not to be significantly affected by subduction processes, which is consistent with the model of Sobolev *et al.* (2000).

Using the parameters described above, the results of the model involving an ancient recycled plagioclase-rich cumulate do not produce isotopic values within the range observed for Fernandina melt inclusions (Fig. 9). For a

Table 2: Inputs for recycled gabbro isotopic evolution

Trace elements[1]	E-DMM[2]	N-DMM[3]	D-DMM[3]
U	0·023	0·0032	0·0018
Th	0·086	0·0079	0·004
Pb	0·075	0·018	0·014
U/Pb	0·3067	0·1778	0·1286
Th/Pb	1·1467	0·4389	0·2857

Isotopes	E-MORB[4]	N-MORB[4]	D-MORB[4]
$^{206}Pb/^{204}Pb$	18·911	18·287	17·462
$^{207}Pb/^{204}Pb$	15·514	15·613	15·341
$^{208}Pb/^{204}Pb$	38·319	38·174	37·025
$^{207}Pb/^{206}Pb$	0·8204	0·8538	0·8785
$^{208}Pb/^{206}Pb$	2·0263	2·0875	2·1203

Gabbro trace elements[5]	Ps[6]	Qs[6]	Os[6]	Hp[6]	GG[7]
U	0·003	0·008	0·043	0·010	0·026
Th	0·013	0·009	0·118	0·030	0·043
Pb	0·163	0·294	0·244	0·160	0·308
U/Pb	0·0184	0·0279	0·1762	0·0625	0·0831
Th/Pb	0·0798	0·0316	0·4836	0·1875	0·1404
Time (Ga)	0·5	1			

[1]In our isotopic calculation, for the back-calculation to the isotopic composition of the gabbro at the time of formation, we tested all of the present-day isotopic values of Pacific MORB marked by the field in Fig. 9. Values below 0·8386 we considered E-MORB and used trace element values listed for E-DMM for the calculation [bound is equal to the average Pacific E-MORB value presented by Donnelly *et al*. (2004)]. Values above 0·8766 we considered D-MORB and used trace element values listed for D-DMM for the calculation (Workman & Hart, 2005). Figure 9 shows the results of calculation using the extreme minimum $^{207}Pb/^{206}Pb$ and $^{208}Pb/^{206}Pb$ ratios for the field (E-MORB), the extreme maximum $^{207}Pb/^{206}Pb$ and $^{208}Pb/^{206}Pb$ of the field (D-MORB), and an average N-MORB isotopic ratio.
[2]Donnelly *et al*. (2004).
[3]Workman & Hart (2005).
[4]Stracke *et al*. (2005).
[5]At time of formation.
[6]Hart *et al*. (1999); Hp, highest U/Pb ratio protolith; Ps, lowest U/Pb ratio strip sample; Qs, lowest Th/Pb ratio strip sample; Os, highest U/Pb and Th/Pb ratio strip sample.
[7]Zimmer *et al*. (1995).

recycled gabbro to evolve to a Fernandina isotopic composition, the present-day MORB isotopic value has to be equal to the most enriched E-MORB in the Pacific Ocean (which has a similar isotopic composition to the Fernandina lavas; Fig. 9) and experience an incredibly short recycling time (≤152 Myr). This would avoid large changes in the initial isotopic composition but requires improbably young recycled material. Alternatively, to stay within the more reasonable minimum age of recycling (500 Ma) we would have to expand the range in present-day MORB isotopic values to include the most enriched samples measured for Atlantic E-MORB, samples that have been affected by the Sierra Leone plume (Schilling *et al*., 1994). The very young age and/or the extreme isotopic composition necessary to reproduce the Fernandina Pb isotope values makes it unlikely that melt inclusions with the ghost plagioclase signature are sampling an ancient recycled plagioclase-rich cumulate in the source of

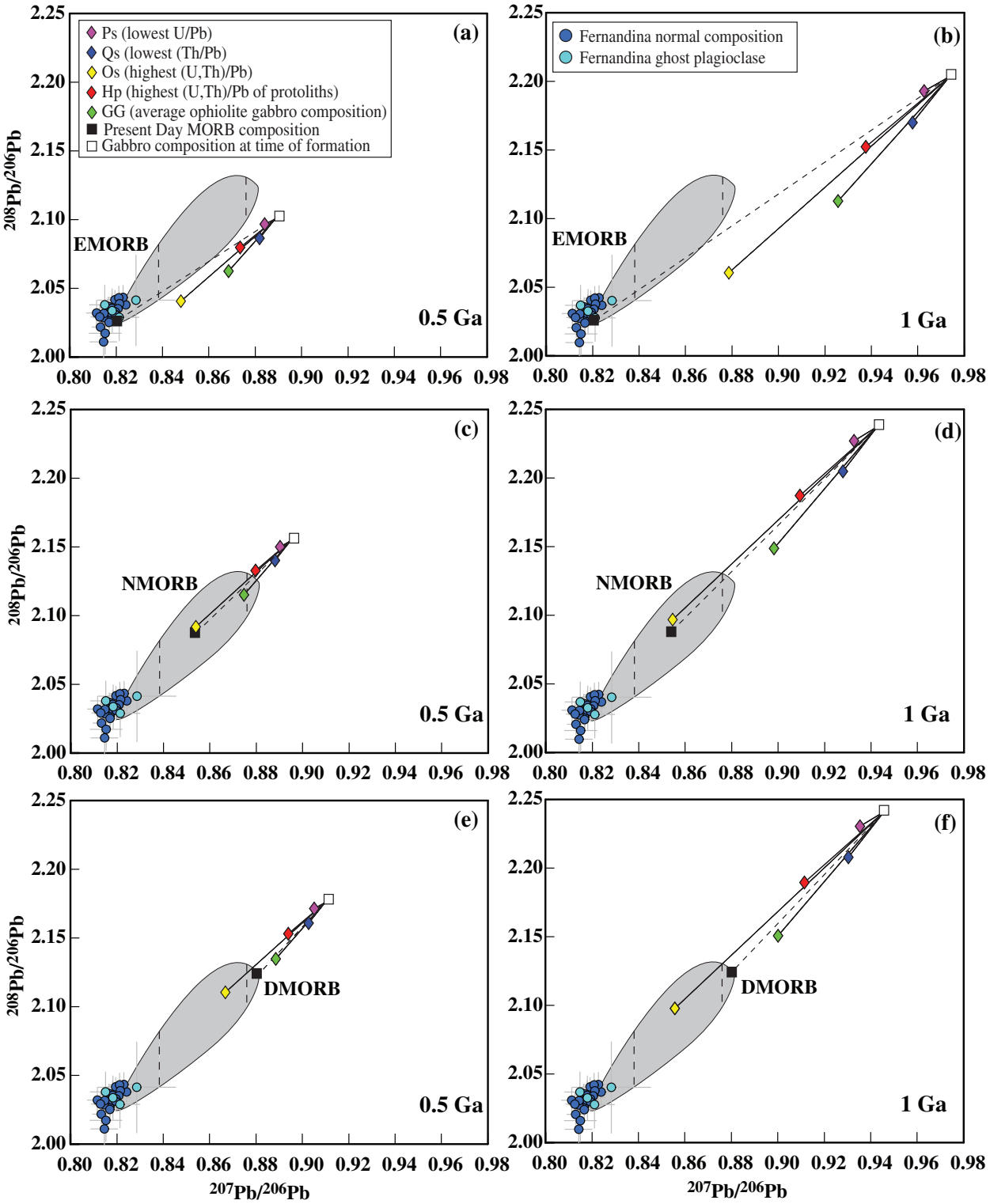

Fig. 9. $^{208}Pb/^{206}Pb$ vs $^{207}Pb/^{206}Pb$ ratios for single melt inclusions from Fernandina Island compared with calculated trends for the isotopic evolution of ancient plagioclase cumulates. The field for MORB (grey shaded) represents a compilation for Pacific MORB (Stracke *et al.*, 2005, and references therein). Vertical dashed lines separate the Pacific MORB field into fields for E-MORB, N-MORB, and D-MORB. Dashed lines show the back-calculation of the present-day $^{208}Pb/^{206}Pb$ and $^{207}Pb/^{206}Pb$ for selected values of the present-day Pacific MORB field (black squares), to an initial isotopic composition at 0·5 Ga (a, c, e) and 1·0 Ga (b, d, f) (white squares). Starting Pacific MORB compositions (black squares) for this calculation are separated into E-MORB (a, b), N-MORB (c, d) and D-MORB (e, f). Continuous lines show the

(continued)

the Galapagos plume. An additional melting–mixing step is needed, which requires us to expand our model to include trace elements in addition to Pb isotopes.

Melting of an ancient plagioclase cumulate: adding Pb isotopes to a critical melting model

To test whether melting of plume mantle containing an ancient recycled plagioclase-rich cumulate could reproduce the trace element and Pb isotopic composition of the Fernandina melt inclusions with the ghost plagioclase signature, we use the model presented by Sobolev *et al.* (2000). The melting reactions, phase proportions and partition coefficients are given in Table 3. This model considers that a quartz-eclogite (recycled plagioclase-rich cumulate) entrained in a mantle plume starts to melt before the surrounding mantle during adiabatic upwelling. The resulting Si-rich melt infiltrates and reacts with the surrounding peridotite to form pyroxene (Yaxley & Green, 1998) transferring the trace element signature of the recycled plagioclase-rich cumulate to the peridotite. The subsequent melting of this hybrid mantle in the garnet stability field could then produce melts characterized by a ghost plagioclase trace element signature (Sobolev *et al.*, 2000).

Although the Fernandina mantle has noble gas consistent with a less degassed mantle composition (FOZO) (Kurz & Geist, 1999), we consider for the modeling two different mantle compositions, a trace element depleted DMM (Workman & Hart, 2005) and a primitive mantle (PM, McDonough & Sun, 1995) to better simulate a large range of possibilities. For the isotope composition of the DMM mantle, we use the Pb isotope composition of DMM from Stracke *et al.* (2005). For the PM mantle we use the average Pb isotopic composition of lavas from Fernandina (Saal *et al.*, 2007). For the remaining parameters (composition of ancient plagioclase, degree of melting of the eclogite, fraction of eclogite melt to peridotite used for mantle hybridization, and the degree of melting of the hybrid mantle) we test a range of values and present the results of the best-fit models in Fig. 10 and Table 4. The ancient recycled plagioclase-rich cumulate isotopic composition is calculated using the method and compositional ranges described in the previous section. The parameters for the cumulate calculation that yield the isotopic composition closest to the Fernandina melt inclusion isotopic compositions are the extreme $^{207}Pb/^{206}Pb$ and $^{208}Pb/^{206}Pb$ of the E-MORB Pacific ridge samples and the composition of either the gabbro strip Os (Hart *et al.*, 1999) or the average Gabal Gerf gabbro composition GG (Zimmer *et al.*, 1995) at an age of 500 Ma and 1 Ga. Following Sobolev *et al.* (2000) we consider that the melting eclogite has a residual porosity of 8%, which is reasonable for a high-Si melt (Yaxley & Green, 1998). Any fraction of melt above 8% will be removed to hybridize the surrounding mantle (either DMM or PM) at a ratio 0·1 melt to 0·9 peridotite. Although we tested our model using 9–50% instantaneous and aggregate eclogite melt, the results presented in Fig. 10 use the first weight per cent past the porosity ($F = 9\%$) of instantaneous melt for hybridization because this produces the largest Sr anomaly. We also varied the proportion of eclogite melt to peridotite from 0·1:0·9 to 0·03:0·97, though this does not produce a significant change from what we show in Fig. 10. Following hybridization, we consider 5–15% accumulated critical melting of the hybrid mantle with 2% porosity. The resulting melt extracted from the mantle is mixed with typical Fernandina melt, in 10% increments. For the composition of the modeled melt originating from the hybrid mantle, differences of between 5 and 15% melting will not significantly affect the Sr/Sr* ratio, therefore we present an average value of 10% melting in Fig. 10. Results of each step of this model for the ideal parameters indicated above are reported in Table 4. None of the models were able to reproduce both the trace element and Pb isotope compositions of the ghost plagioclase inclusions. Over the range of tested parameters, the percentage of the eclogite needed to create the ghost plagioclase trace element signature forces the Pb isotopes outside the measured range of the Fernandina inclusions with ghost plagioclase signature.

Present-day formation of a ghost plagioclase signature

To explain the similar Pb isotopic composition of the Fernandina melt inclusions with and without the ghost plagioclase the process forming the ghost plagioclase signature must create both the observed trace element anomalies and isotopic ratios. For example, a plagioclase cumulate formed in the oceanic crust beneath Fernandina within the last few million years would have the present-day Pb isotope composition of Fernandina lavas. Therefore, a shallow-level diffusive interaction of a Fernandina melt with this plagioclase-rich cumulate

Fig. 9 Continued
evolution of the recycled gabbro to its present-day isotopic composition for several gabbro compositions. The gabbros chosen represent the extreme compositions of (U, Th)/Pb ratios from the compositions reported by Hart *et al.* (1999). Also included is the average gabbro composition of the Gabal Gerf ophiolite (Zimmer *et al.*, 1995). Single gabbro compositions are indicated by diamonds of different colours. For the back-calculation to the isotopic composition of the gabbro at the time of formation, we tested all of the present-day isotopic compositions of Pacific MORB within the grey field, but have included only the results of calculations using the extreme minimum value of $^{207}Pb/^{206}Pb$ and $^{208}Pb/^{206}Pb$ for the E-MORB field, the extreme maximum $^{207}Pb/^{206}Pb$ and $^{208}Pb/^{206}Pb$ of the D-MORB field and an average N-MORB isotopic composition, as these represent the boundaries of the calculation. It should be noted that the results of all six models are well outside the field defined by the Fernandina melt inclusions. Model input data are given in Table 2.

Table 3: Partition coefficients, mineral modes and parameters used in critical melting model

Element	K_d solid–melt[1]				
	Ol	Opx	Cpx	Gt	Co
Ba	0·000005	0·000006	0·0003	0·00007	0
Th	0·000007	0·00002	0·0021	0·0021	0
Nb	0·00005	0·003	0·0089	0·011	0
K	0·00002	0·0001	0·001	0·01	0
La	0·0002	0·0031	0·054	0·0007	0
Sr	0·00004	0·0007	0·091	0·0007	0
Ce	0·00007	0·0021	0·086	0·0026	0
Nd	0·0003	0·0023	0·19	0·027	0
Zr	0·001	0·012	0·26	0·2	0
Sm	0·0009	0·0037	0·27	0·22	0
Eu	0·0005	0·009	0·43	0·61	0
Ti	0·015	0·086	0·4	0·6	0
Dy	0·0027	0·011	0·44	2	0
Y	0·0082	0·015	0·47	2	0
Er	0·0109	0·021	0·39	3·3	0
Yb	0·024	0·038	0·43	6·4	0
Pb	0·0003	0·0014	0·0075	0·0003	0
Eclogite melting					
start mode[2]	0	0	0·4	0·5	0·1
Melting mode[3]	0	0	0·6	0·1	0·3
α[4]	0·08				
F(instant)[5]	0·09				
Lherzolite melting[6]					
Reaction	−1·1	0·5	0·8	−0·2	0
Start mode	0·53	0·14	0·265	0·065	0
Melting mode	0·1	−0·3	1	0·2	0
α[4]	0·02				
F(aggre)[7]	0·1				

[1]Halliday *et al*. (1995) except for quartz (coesite) where partition coefficients were assumed to be zero.
[2]Estimated using the thermodynamic model of Sobolev & Babeyko (1994).
[3]Taken from the experiments of Yaxley & Green (1998).
[4]Porosity of the melting model. Represents the amount of melt retained by the solid matrix to prevent compaction.
[5]Amount of instantaneous, eclogite melt extracted that hybridizes the overlying mantle.
[6]The reaction coefficients represent the factors for each mineral that are multiplied by the fraction of eclogite melt to determine the amount those minerals are added or subtracted from the original mantle peridotite to obtain the mineral proportions of the hybridized mantle (Sobolev & Babeyko, 1994;Yaxley & Green, 1998; Sobolev *et al*., 2000). The model results presented in Fig. 10 use 0·1 as the fraction of eclogite melt to represent a 0·1:0·9 proportion of eclogite melt to peridotite. Quantitative modeling of the phase change that occurs during this reaction has been given by Sobolev *et al*. (2000). The starting mode for the lherzolite melting is taken from Hofmann (1988). This starting mode will change depending on the amount of melt created during eclogite melting. The melting mode was taken from Sobolev *et al*. (2000).
[7]Amount of aggregate melt extracted from the hybrid mantle, hypothesized by Sobolev *et al*. (2000) to ultimately form the ghost plagioclase signature.

would create the needed trace element anomalies while not affecting the Pb isotopes and the major element composition of the melt. To illustrate this, we have included a simple diffusion model that considers the approximate solution to the diffusion equations in a finite crystal–melt geometry (Hart, 1993) presented by Saal *et al*. (2007) (Fig. 11). This model considers an end-member case of melt percolating through a troctolite mush with equal proportions of plagioclase and olivine. For simplicity, we neglect the effects of crystal dissolution and precipitation that may occur during diffusive re-equilibration of a partially molten system (Hart, 1993; Liang, 2003); that is, we assume the melt is in major element equilibrium with the plagioclase cumulate (Saal *et al*., 2007). As a result, because of the low trace element budget of olivine, variations in the trace element content of the melt are due solely to diffusive exchange between plagioclase and melt.

There are two values for melt concentration that we must consider: the melt from which the plagioclase cumulate originally crystallizes and the composition of the melt interacting with the cumulate. The geochemistry of the Fernandina melt inclusions with ghost plagioclase signature (large positive Sr/Sr*, large range in Nb/La ratio, and Pb isotope composition similar to those of the Fernandina whole-rocks) limits what these melt compositions can be. A large positive Sr anomaly, as is observed in the Fernandina melt inclusions with the ghost plagioclase signature, can be created by diffusion if the melt from which the plagioclase originally crystallized was much more enriched in trace elements than the percolating melt. Therefore, for the cumulate composition, we considered the crystallization of plagioclase from an evolved Fernandina melt (AHA31A; Geist *et al*., 2006) and we assume a Pb isotopic composition equivalent to that of the Fernandina whole-rocks (Saal *et al*., 2007). For the percolating melt we considered a trace element depleted melt because the Nb/La ratio in the depleted Fernandina melt inclusions with and without plagioclase ghost signature is much lower than those of the 'normal' inclusions (Figs 6 and 11). Although part of the Nb/La variation can be reproduced by the diffusive interaction of a percolating melt with the plagioclase cumulate owing to the different diffusivity of Nb and La in plagioclase (Cherniak, 2003; Saal & Van Orman, 2004), the total variation in Nb/La ratio cannot be reproduced using reasonable parameters, suggesting that the percolating melt is depleted (i.e. low Nb/La). Therefore, for the percolating melt composition, we assumed a 12% aggregated fractional melt of the DMM composition (Workman & Hart, 2005) with a Nb/La ratio of 0·773 and with the average isotopic composition of Pacific MORB (Stracke *et al*., 2005). Although we do not observe erupted lavas with trace element depleted compositions on Fernandina, the trace element depleted melt inclusions suggest the presence of a low-volume, trace

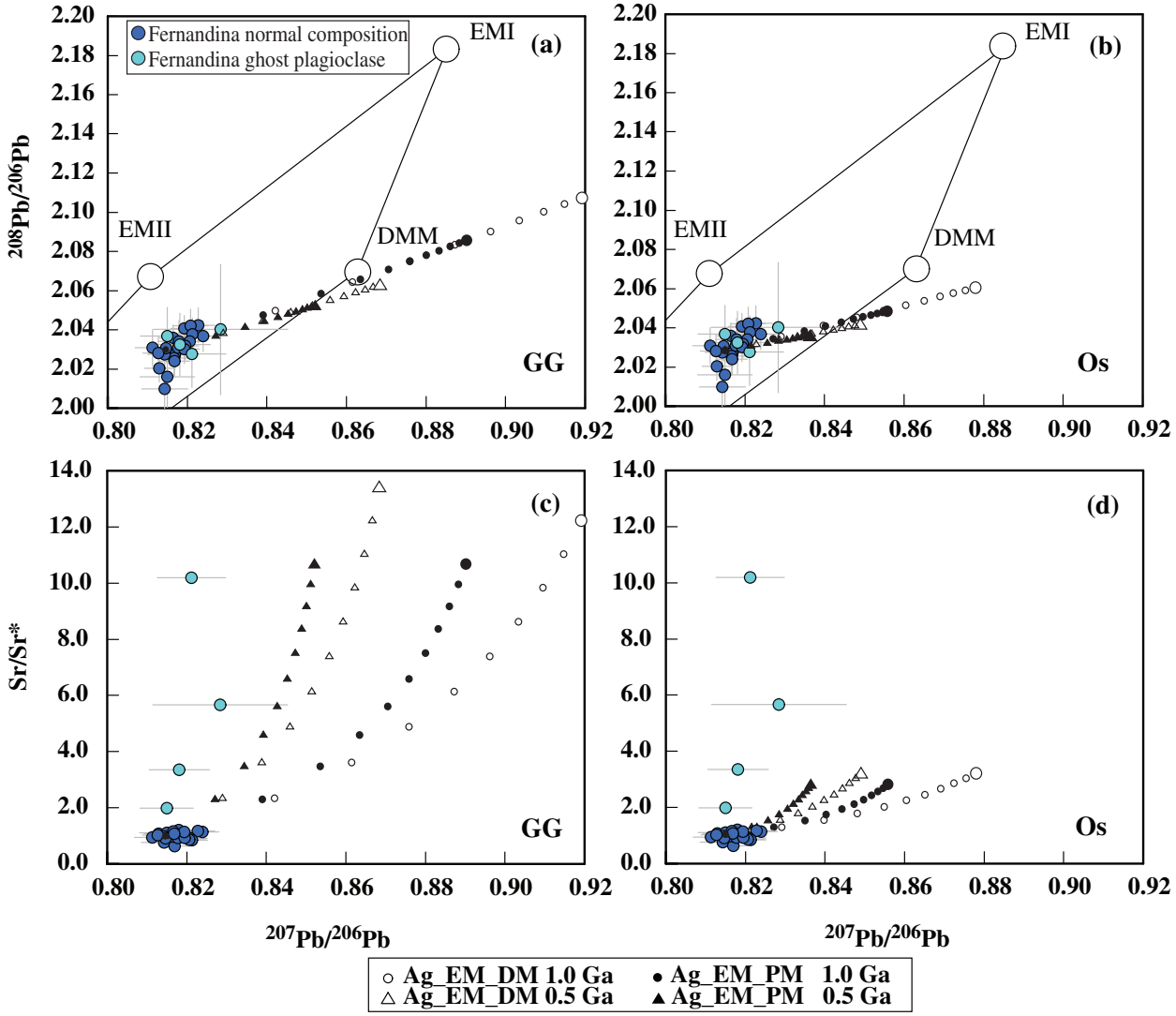

Fig. 10. Comparison of Fernandina melt inclusion compositions with trends produced by mixing of a typical Fernandina basalt with melts generated by partial melting of a mantle plume containing an ancient (~0·5–1 Ga) recycled plagioclase-rich cumulate. (a, b) $^{208}Pb/^{206}Pb$ vs $^{207}Pb/^{206}Pb$. Large open circles are the end-members from the mantle tetrahedron projected onto the $^{208}Pb/^{206}Pb$–$^{207}Pb/^{206}Pb$ plane (Hart, 1988; Hart *et al.*, 1992; Hauri *et al.*, 1994; Workman *et al.*, 2004; Stracke *et al.*, 2005). (c, d) Sr/Sr* vs $^{207}Pb/^{206}Pb$. Results are shown of a critical melting model using DMM (black open symbols) and PM mantle source compositions (black filled symbols) hybridized with ancient recycled plagioclase cumulates (now eclogite) formed at 0·5 Ga (triangles) and 1 Ga (circles) (model results are reported in Table 4). (See text for details.) The parameters of the calculation are, for the starting composition, the extreme $^{207}Pb/^{206}Pb$ and $^{208}Pb/^{206}Pb$ of E-MORB Pacific samples and the two gabbro compositions that resulted in Pb isotope ratios closest to Fernandina: (a, c) ancient cumulate composition calculated using the Gabal Gerf average gabbro composition GG (Zimmer *et al.*, 1995), and (b, d) ancient cumulate using the Os strip gabbro composition (Hart *et al.*, 1999). The model trends represent mixing of 10% aggregated critical melt of the hybrid mantle (Ag.EM.DM or Ag.EM.PM) with normal Fernandina basalt in 10% increments (see text for explanation of the model). End-members of the hybrid mantle melt used for mixing (results of the critical melting model) are indicated by a larger symbol; smaller symbols denote 10% mixing steps. It should be noted that the Pb isotope ratios and the Sr/Sr* cannot be simultaneously reproduced by this model.

element depleted melt composition in the plumbing system of this volcano.

In a crystal mush zone, either in a shallow crustal magma chamber or shallow regions of the mantle, melt is expected to percolate by both reactive porous flow (low melt/rock ratio more susceptible to diffusive interaction with the crystal cumulate) and channelized melt flow (high melt/rock ratio where the composition of the melt is similar to the erupted lavas) (e.g. Jaupart & Tait, 1995; Kelemen *et al.*, 1995). Therefore in a mush zone beneath Fernandina we might expect the presence of two melts (produced by channelized and reactive porous flow), which will progressively aggregate as shown in Fig. 11, reproducing the correlation between Nb/La and

Table 4: Starting compositions and results of critical melting model

Element	Starting compositions				Modeling results			
	Gabbro: Os	9% EM	DM	PM	10/90 EM–DM	10/90 EM–PM	10% Ag–EM–DM	10% Ag–EM–PM
Ba	2·46	26·70	0·56	6·60	3·18	8·61	38·23	103·63
Th	0·12	1·26	0·01	0·08	0·13	0·20	1·60	2·38
Nb	0·76	7·58	0·15	0·66	0·89	1·35	10·60	16·05
K	500·04	5148·60	49·81	240·00	559·70	730·90	6725·00	8781·80
La	1·19	10·76	0·19	0·65	1·25	1·66	13·78	18·31
Sr	155·64	1264·10	7·66	19·90	133·30	144·30	1365·10	1477·90
Ce	4·50	36·78	0·55	1·68	4·17	5·19	43·09	53·54
Nd	3·51	20·67	0·58	1·25	2·59	3·19	21·13	26·04
Zr	19·00	68·20	5·08	10·50	11·39	16·27	76·79	109·65
Sm	1·23	4·21	0·24	0·41	0·64	0·79	4·24	5·25
Eu	0·53	0·98	0·10	0·15	0·18	0·24	0·89	1·14
Ti	1865·53	3565·70	716·30	1205·00	1001·20	1441·10	4547·80	6545·60
Dy	0·00	0·82	0·51	0·67	0·54	0·69	2·10	2·69
Y	12·70	10·29	3·33	4·30	4·02	4·90	15·07	18·34
Er	0·00	0·33	0·35	0·44	0·35	0·43	1·20	1·48
Yb	1·28	0·38	0·37	0·44	0·37	0·43	0·90	1·06
Pb	0·24	2·58	0·02	0·15	0·27	0·39	3·27	4·69
	0·5 Ga				*0·5 Ga*	*0·5 Ga*		
$^{207}Pb/^{206}Pb$	0·8479		0·8626	0·8147	0·8488	0·8362		
$^{208}Pb/^{206}Pb$	2·0405		2·0687	2·0291	2·0422	2·0365		
	1 Ga				*1 Ga*	*1 Ga*		
$^{207}Pb/^{206}Pb$	0·8788				0·8778	0·8556		
$^{208}Pb/^{206}Pb$	2·0606				2·0611	2·0491		

Element	Starting compositions				Modeling results			
	Gabbro: GG	9% EM	DM	PM	10/90 EM–DM	10/90 EM–PM	10% Ag–EM–DM	10% Ag–EM–PM
Ba	47·44	514·86	0·56	6·60	51·99	57·43	625·81	691·21
Th	0·04	0·46	0·01	0·08	0·05	0·12	0·64	1·42
Nb	0·73	7·26	0·15	0·66	0·86	1·32	10·22	15·67
K	1577·19	16239·30	49·81	240·00	1668·80	1839·90	20051·40	22108·10
La	1·33	12·06	0·19	0·65	1·38	1·79	15·21	19·74
Sr	561·77	4562·80	7·66	19·90	463·20	474·20	4742·90	4855·70
Ce	3·81	31·11	0·55	1·68	3·61	4·62	37·23	47·68
Nd	2·56	15·07	0·58	1·25	2·03	2·63	16·56	21·48
Zr	15·30	54·92	5·08	10·50	10·07	14·94	67·84	100·70
Sm	0·72	2·46	0·24	0·41	0·46	0·61	3·08	4·08
Eu	0·52	0·96	0·10	0·15	0·18	0·23	0·88	1·13
Ti	5214·78	9967·30	716·30	1205·00	1641·40	2081·20	7455·50	9453·30
Dy	0·95	0·78	0·51	0·67	0·53	0·68	2·08	2·68
Y	6·48	5·25	3·33	4·30	3·52	4·40	13·18	16·46
Er	0·53	0·29	0·35	0·44	0·34	0·42	1·18	1·47
Yb	0·45	0·13	0·37	0·44	0·34	0·41	0·84	1·00
Pb	0·31	3·25	0·02	0·15	0·34	0·46	4·08	5·49
	0·5 Ga				*0·5 Ga*	*0·5 Ga*		

(continued)

Table 4: Continued

Element	Starting compositions				Modeling results			
	Gabbro: GG	9% EM	DM	PM	10/90 EM__DM	10/90 EM__PM	10% Ag__EM__DM	10% Ag__EM__PM
$^{207}Pb/^{206}Pb$	0·8685		0·8626	0·8147	0·8682	0·852		
$^{208}Pb/^{206}Pb$	2·0624		2·0687	2·0291	2·0627	2·0521		
	1 Ga				*1 Ga*	*1 Ga*		
$^{207}Pb/^{206}Pb$	0·9258				0·9225	0·8899		
$^{208}Pb/^{206}Pb$	2·1124				2·1101	2·0855		

Gabbro: starting plagioclase cumulate composition used for eclogite melting (Os, Hart *et al.*, 1999; GG, Zimmer *et al.*, 1995). 9%EM is the result of 9% instantaneous melting of eclogite. DM, depleted mantle composition (Workman & Hart, 2005); PM, primitive mantle composition (McDonough & Sun, 1995). 10/90 EM__DM is composition of 10% eclogite melt, 90% DM forming a hybrid mantle; 10/90 EM__PM is composition of 10% eclogite melt, 90% PM forming a hybrid mantle; 10% Ag__EM__DM are results of 10% aggregate melting of hybrid eclogite melt–DM mantle; 10% Ag__EM__PM are results of 10% aggregate melting of hybrid eclogite melt–PM mantle. Also shown are the resulting Pb isotope ratios of the hybrid mantle for plagioclase cumulates formed at 0·5 and 1 Ga. The Pb isotope composition of DM is from Stracke *et al.*, (2005), whereas the Pb isotope composition of the PM mantle is taken to be equivalent to typical Fernandina basalt (Saal *et al.*, 2007). Results of the melting of the hybrid mantle (both DM and PM) are shown in Fig. 10.

Sr/Sr* that is observed in the ghost plagioclase melt inclusions.

Other parameters include temperature, crystal size and melt to rock ratio. Based on the results of previous studies of the crust–mantle transition zone we set a temperature of 1200°C, a grain size of 1 mm and a melt to rock ratio of 1% (Boudier *et al.*, 1996; Dunn *et al.*, 2001). We further assume the temperature is constant, which is consistent with inefficient heat removal from the crust–mantle transition zone (Dunn *et al.*, 2001). For the model we assume that the solid is homogeneous at the onset of diffusion. We also assume that the concentration in the middle of the grains is controlled by diffusion and that the mineral grains do not deform. Diffusion in the melt is considered instantaneous and the boundary between solid and melt is assumed to be in chemical equilibrium at all times [see Saal *et al.* (2007) for further considerations]. The values of all parameters used are given in Table 5.

The results of this model (Fig. 11) demonstrate how the ghost plagioclase signature can be produced by diffusive interaction between a depleted melt and a plagioclase cumulate followed by subsequent mixing of the reacted melt with a normal composition Fernandina melt. The diffusivities of Sr and Pb, along with those of Ba, K and Eu^{2+}, are several orders of magnitude faster than those for the other trace elements (e.g. Th, Nb and REE), allowing the melt to develop a plagioclase-rich signature within a short amount of time (Behrens *et al.*, 1990; Cherniak & Watson, 1994; Giletti & Casserly, 1994; Cherniak, 1995, 2002, 2003; Giletti & Shanahan, 1997; Saal & Van Orman, 2004). The fast diffusion of Pb also causes the rapid change in the Pb isotope composition of the melt from the initial DMM value to a value within the range of the Fernandina basalts. The rapid re-equilibration of the Pb isotope composition of the melt, however, necessitates that the plagioclase cumulates have the same Pb isotope composition as the Fernandina basalts. If we consider the opposite situation, in which the plagioclase cumulate originated from a magma with a trace element and isotopic composition similar to typical N-MORB (i.e. crust created at the Galapagos Spreading Center), and the percolating melt has the isotopic and trace element composition of normal Fernandina basalts, the result will be a melt with the isotopic composition of N-MORB and a negative Sr anomaly, thus not reproducing either the Pb isotopes or the trace element characteristics of the melt inclusions with ghost plagioclase signature. Alternatively, although unlikely, the plagioclase-rich cumulates formed at the ridge now under Fernandina might have had the extreme E-MORB composition found in the Pacific Ocean, as this is similar to Fernandina whole-rocks. However, there is no evidence to support the existence of an extreme E-MORB composition in the lithosphere beneath Fernandina.

It is clear that our simple model cannot reproduce the signature of the melt inclusion with the highest Sr/Sr* (D25C-2-29), but our model is limited by only considering diffusion. Burgess *et al.* (in preparation) explored an expansion of this model that includes dissolution–precipitation of plagioclase in addition to kinetic equilibration. The additional processes expand the number of starting compositions that allow present-day interaction between melt and plagioclase cumulates to result in a ghost plagioclase signature and further highlight how interaction provides the simplest explanation for the creation of a ghost plagioclase signature in the Galapagos Archipelago.

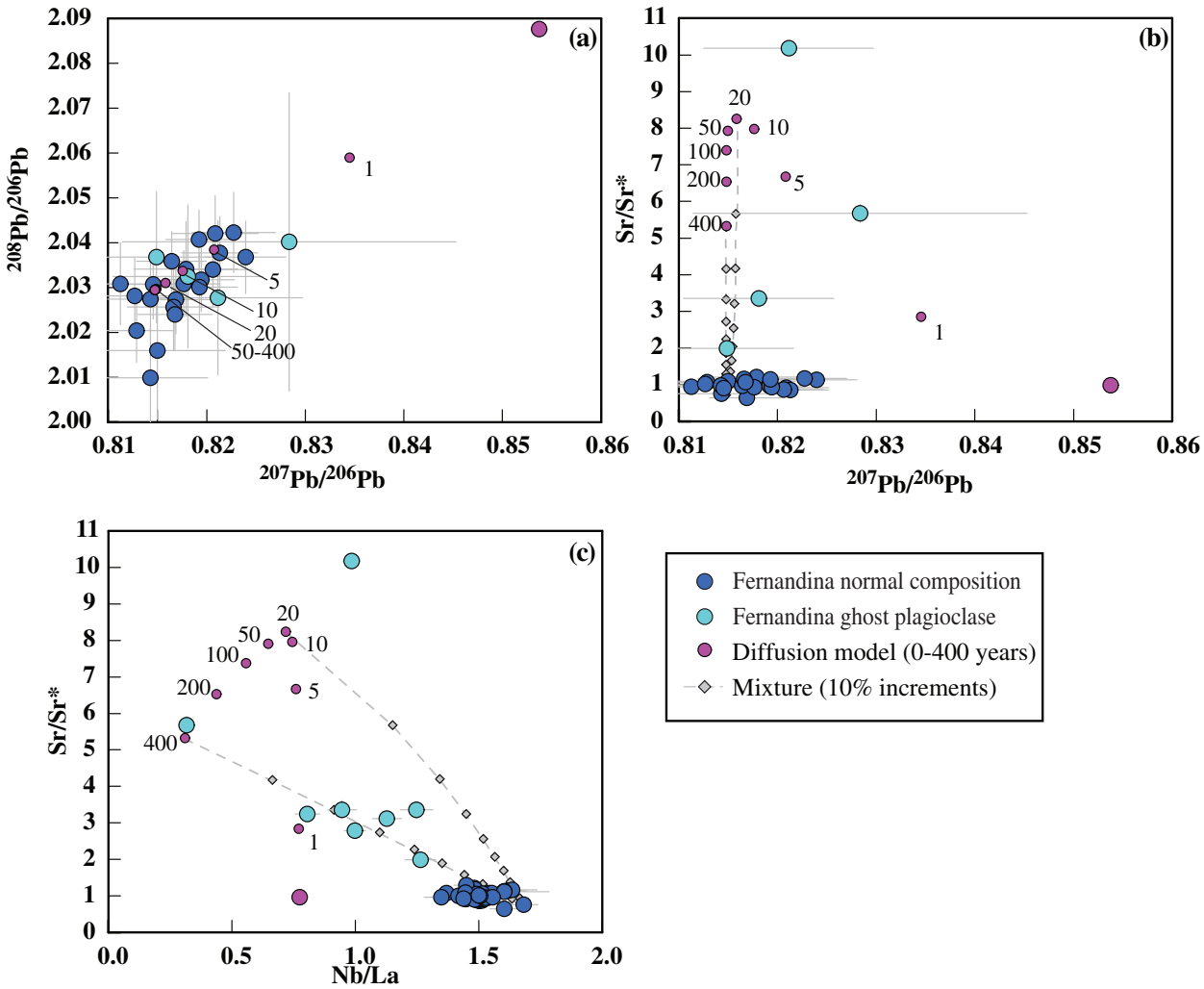

Fig. 11. Comparison of Fernandina melt inclusion compositions with trends produced by diffusively reacting a 12% aggregated, fractional melt generated from a DMM source (Workman & Hart, 2005) with a plagioclase cumulate created from an evolved Fernandina melt (AHA3lA, Geist *et al.*, 2006) at 1200°C (see text for the description of the model and Table 5 for the model parameters). (a) $^{208}Pb/^{206}Pb$ vs $^{207}Pb/^{206}Pb$; (b) Sr/Sr* vs $^{207}Pb/^{206}Pb$; (c) Sr/Sr* vs Nb/La. Large purple circle indicates the composition of the percolating melt. Small purple circles represent the composition of the melt as diffusive equilibration with the plagioclase-rich cumulate progresses within a range of 1–400 years indicated by the numbers next to the small circles. Grey dashed lines represent mixing between the normal Fernandina basalt (D25C-2-19B) and the percolating melt that reacted over 20 and 400 years; the grey diamonds denote 10% mixing steps.

Presence of the ghost plagioclase signature in settings outside the Galapagos

The ghost plagioclase signature is a well-documented phenomenon that, despite occurring in only a small percentage of samples, can be found in multiple ocean island basalt (OIB) suites (Gurenko & Chaussidon, 1995; Hofmann & Jochum, 1996; Yang *et al.*, 1998; Chauvel & Hemond, 2000; Sobolev *et al.*, 2000; Kent *et al.*, 2002; Huang *et al.*, 2005; Ren *et al.*, 2005; Maclennan, 2008) and MORB (Kamenetsky *et al.*, 1998; Danyushevsky *et al.*, 2003, 2004). However, very few studies have reported Pb isotopes in addition to trace and major elements. The study of Maclennan (2008) reported Pb isotopes for a suite of Icelandic melt inclusions with several inclusions identified as having the ghost plagioclase signature. The Pb isotope compositions of the anomalous melt inclusions are within the range of Pb isotope ratios measured for normal composition inclusions. This led the authors to conclude that the ghost plagioclase inclusions were sampling a present-day process as opposed to an ancient recycled gabbro component in the mantle source, consistent with the findings of our study. The study of Sobolev *et al.* (2011) reported both Sr and Pb isotope data for a suite of melt inclusions from Hawaii that includes several inclusions with large positive Sr anomalies in primitive mantle normalized trace element patterns.

Table 5: Diffusion model

	K_d (plag–melt)[1]	D_{plag} (1200°C, $m^2\ s^{-1}$)[2]	Plagioclase melt[3]	Initial melt[4]	PM normalized output data[5]							
					1 years	5 years	10 years	20 years	50 years	100 years	200 years	400 years
Ba	0·230	8·09E − 19	271	4·69	0·75	0·88	1·06	1·40	2·41	4·03	7·04	9·79
Th	0·050	3·10E − 21	2·88	0·07	0·83	0·83	0·83	0·83	0·83	0·84	0·84	0·84
U	0·024	3·10E − 21	0·98	0·03	1·31	1·31	1·31	1·31	1·31	1·32	1·32	1·32
Nb	0·030	3·10E − 21	47·9	1·24	1·88	1·88	1·88	1·88	1·88	1·88	1·89	1·89
Ta	0·030	3·10E − 21	3·42	0·08	2·16	2·16	2·16	2·16	2·16	2·17	2·17	2·17
K	0·171	4·38E − 16	14693·6	408·33	18·79	47·21	53·76	54·84	54·86	54·86	54·86	54·86
La	0·106	3·87E − 19	35·14	1·60	2·48	2·52	2·57	2·67	2·96	3·44	4·39	5·32
Ce	0·081	3·87E − 19	79·68	4·57	2·73	2·76	2·79	2·86	3·05	3·38	4·01	4·64
Pb	0·511	1·41E − 17	2·48	0·15	1·84	4·76	7·57	11·25	15·11	15·89	15·94	15·94
Pr	0·104		10·8	0·88	3·27	3·29	3·32	3·37	3·52	3·77	4·27	4·76
Sr	1·813	3·37E − 17	561	63·48	9·34	21·99	26·50	27·83	27·91	27·91	27·91	27·91
Nd	0·084	2·92E − 19	44·96	4·76	3·81	3·83	3·85	3·88	3·99	4·17	4·53	4·88
Zr	0·004	3·10E − 21	350	41·47	3·95	3·95	3·95	3·95	3·95	3·95	3·95	3·95
Hf	0·015	3·10E − 21	7·55	1·27	4·50	4·50	4·50	4·50	4·50	4·50	4·50	4·50
Sm	0·056	2·92E − 19	10·27	1·88	4·62	4·63	4·63	4·65	4·70	4·77	4·93	5·08
Eu	0·534	2·92E − 19	3·19	0·74	5·43	7·51	9·29	11·21	12·64	13·01	13·53	14·00
Ti	0·076	3·10E − 21	24932·9	5310·42	4·41	4·41	4·41	4·41	4·41	4·41	4·41	4·41
Gd	0·017		9·65	2·68	5·04	5·04	5·05	5·05	5·08	5·12	5·19	5·27
Tb	0·038		1·43	0·49	5·25	5·25	5·25	5·25	5·27	5·29	5·32	5·36
Dy	0·019	3·24E − 19	7·78	3·37	5·46	5·46	5·46	5·46	5·46	5·46	5·46	5·46
Er	0·012		3·88	2·12	5·04	5·04	5·04	5·04	5·04	5·05	5·05	5·05
Yb	0·015	5·06E − 19	3·16	2·04	4·63	4·63	4·63	4·63	4·63	4·64	4·65	4·65
$^{207}Pb/^{206}Pb$			0·8147	0·8538	0·8345	0·8208	0·8176	0·8159	0·8150	0·8148	0·8148	0·8148
$^{208}Pb/^{207}Pb$			2·0291	2·0875	2·0587	2·0382	2·0334	2·0308	2·0294	2·0292	2·0292	2·0292

Grain size of plagioclase is 0.001 (m); %melt to solid is 1%; %Plag in solid is 50%.
[1]Experimentally determined partition coefficients for plagioclase (An_{80}) at 1200°C from Bedard (2006).
[2]Diffusion coefficients from Cherniak & Watson (1994), Giletti & Casserly (1994), Cherniak (1995, 2002, 2003) and Giletti & Shanahan (1997) for plagioclase at 1200°C. For diffusion coefficients not determined experimentally we used estimates based on cation size and charge (Behrens *et al.*, 1990; Saal & Van Orman, 2004). We assumed that the diffusion coefficients for Nb, Ta, Zr, Hf, and Ti are similar to those of Th and U. We assumed Eu is 50% Eu^{2+} and that the diffusion coefficient for Eu^{2+} is similar to that of Sr.
[3]Geist *et al.* (2006) composition AHA31A with isotopic composition of average Fernandina whole-rock.
[4]The 12% aggregated fractional melt of DMM composition from Workman & Hart (2005) with the isotopic values of average Pacific DMM from Stracke *et al.* (2005).
[5]McDonough & Sun (1995).

The inclusions with the Sr anomalies did not fall outside the Sr and Pb isotopic range defined by the inclusions with normal compositions; however, the Sr anomaly correlates positively with Al_2O_3 content, suggesting shallow-level interaction between melts and plagioclase-rich cumulates in the present-day oceanic lithosphere beneath Hawaii. These few examples indicate that without the Pb or any other isotope data for the melt inclusions, it is difficult to unequivocally prove a recycled origin for the ghost plagioclase signature.

CONCLUSIONS

The major and trace element concentrations unique to the 'ghost plagioclase' signature can be re-created equally well by models that involve plagioclase-rich cumulates either as an ancient recycled oceanic crustal component in the mantle or as a present-day component in the oceanic lithosphere (Sobolev *et al.*, 2000; Danyushevsky *et al.*, 2003, 2004). Because these two processes require vastly different amounts of time, the Pb isotope data provide an excellent tool for evaluating these distinct models. Pb isotope data

for Galapagos basalts and melt inclusions suggest that the origin of the ghost plagioclase signature in basalts from the Galapagos Archipelago is not produced by the sampling of an ancient (~0·5–1 Ga) recycled plagioclase-rich cumulate within the mantle. Instead, the trace element and Pb isotope data are most consistent with recent interaction between mantle-derived melts and plagioclase-rich cumulates in the oceanic lithosphere. These results demonstrate that careful evaluation of the isotopic compositions of basalts and melt inclusions is required before unusual trace element anomalies such as those for Sr, Ba and Eu can be used to argue for the presence of ancient recycled crust in oceanic basalts.

ACKNOWLEDGEMENTS

We thank K. Kobayashi for his help in understanding the details associated with Pb isotope analysis performed by SIMS at Okayama University. We thank J. Blusztajn for providing the isotopic measurements of AHA D25C host glass, and Tabb Prissel for the reading of the paper. We also thank D. Geist and S. Huang for their thoughtful reviews.

FUNDING

This work was supported by the National Science Foundation Graduate Research Fellowship (Grant No. DGE-1058262 to M.E.P.) and the National Science Foundation Division of Ocean Sciences (Grant No. 0962195).

SUPPLEMENTARY DATA

Supplementary data for this paper are available at *Journal of Petrology* online.

REFERENCES

Allan, J. F. & Simkin, T. (2000). Fernandina Volcano's evolved, well-mixed basalts: Mineralogical and petrological constraints on the nature of the Galapagos plume. *Journal of Geophysical Research—Solid Earth* **105**, 6017–6041.

Baitis, H. W. & Swanson, F. J. (1976). Ocean rise-like basalts within the Galapagos Archipelago. *Nature* **259**, 195–197.

Becker, H., Jochum, K. P. & Carlson, R. W. (2000). Trace element fractionation during dehydration of eclogites from high-pressure terranes and the implications for element fluxes in subduction zones. *Chemical Geology* **163**, 65–99.

Bedard, J. H. (2006). Trace element partitioning in plagioclase feldspar. *Geochimica et Cosmochimica Acta* **70**, 3717–3742.

Behrens, H., Johannes, W. & Schmalzried, H. (1990). On the mechanisms of cation diffusion-processes in ternary feldspars. *Physics and Chemistry of Minerals* **17**, 62–78.

Blichert-Toft, J. & White, W. M. (2001). Hf isotope geochemistry of the Galapagos Islands. *Geochemistry, Geophysics, Geosystems* **2**, 1043.

Boudier, F., Nicolas, A. & Ildefonse, B. (1996). Magma chambers in the Oman ophiolite: Fed from the top and the bottom. *Earth and Planetary Science Letters* **144**, 239–250.

Bow, C. S. & Geist, D. J. (1992). Geology and petrology of Floreana Island, Galapagos Archipelago, Ecuador. *Journal of Volcanology and Geothermal Research* **52**, 83–105.

Chauvel, C. & Hemond, C. (2000). Melting of a complete section of recycled oceanic crust: Trace element and Pb isotopic evidence from Iceland. *Geochemistry, Geophysics, Geosystems* **1**, 1001.

Chauvel, C., Marini, J. C., Plank, T. & Ludden, J. N. (2009). Hf–Nd input flux in the Izu–Mariana subduction zone and recycling of subducted material in the mantle. *Geochemistry, Geophysics, Geosystems* **10**, Q01001.

Cherniak, D. J. (1995). Diffusion of lead in plagioclase and K-Feldspar—An investigation using Rutherford backscattering and resonant nuclear-reaction analysis. *Contributions to Mineralogy and Petrology* **120**, 358–371.

Cherniak, D. J. (2002). Ba diffusion in feldspar. *Geochimica et Cosmochimica Acta* **66**, 1641–1650.

Cherniak, D. J. (2003). REE diffusion in feldspar. *Chemical Geology* **193**, 25–41.

Cherniak, D. J. & Watson, E. B. (1994). A study of strontium diffusion in plagioclase using Rutherford backscattering spectroscopy. *Geochimica et Cosmochimica Acta* **58**, 5179–5190.

Danyushevsky, L. V. (2001). The effect of small amounts of H_2O crystallisation of mid-ocean ridge and backarc basin magmas. *Journal of Volcanology and Geothermal Research* **110**, 265–280.

Danyushevsky, L. V. & Plechov, P. (2011). Petrolog3: Integrated software for modeling crystallization processes. *Geochemistry, Geophysics, Geosystems* **12**, Q07021.

Danyushevsky, L. V., Perfit, M. R., Eggins, S. M. & Falloon, T. J. (2003). Crustal origin for coupled 'ultra-depleted' and 'plagioclase' signatures in MORB olivine-hosted melt inclusions: evidence from the Siqueiros Transform Fault, East Pacific Rise. *Contributions to Mineralogy and Petrology* **144**, 619–637.

Danyushevsky, L. V., Leslie, R. A. J., Crawford, A. J. & Durance, P. (2004). Melt inclusions in primitive olivine phenocrysts: The role of localized reaction processes in the origin of anomalous compositions. *Journal of Petrology* **45**, 2531–2553.

Donnelly, K. E., Goldstein, S. L., Langmuir, C. H. & Spiegelman, M. (2004). Origin of enriched ocean ridge basalts and implications for mantle dynamics. *Earth and Planetary Science Letters* **226**, 347–366.

Dunn, R. A., Toomey, D. R., Detrick, R. S. & Wilcock, W. S. D. (2001). Continuous mantle melt supply beneath an overlapping spreading center on the East Pacific Rise. *Science* **291**, 1955–1958.

Geist, D., White, W. M., Albarède, F., Harpp, K., Reynolds, R., Blichert-Toft, J. & Kurz, M. D. (2002). Volcanic evolution in the Galápagos: The dissected shield of Volcan Ecuador. *Geochemistry, Geophysics, Geosystems* **3**, 1061.

Geist, D. J., Fornari, D. J., Kurz, M. D., Harpp, K. S., Soule, S. A., Perfit, M. R. & Koleszar, A. M. (2006). Submarine Fernandina: Magmatism at the leading edge of the Galapagos hot spot. *Geochemistry, Geophysics, Geosystems* **7**, Q12007.

Gibson, S. A., Geist, D. G., Day, J. A. & Dale, C. W. (2012). Short wavelength heterogeneity in the Galapagos plume: Evidence from compositionally diverse basalts on Isla Santiago. *Geochemistry, Geophysics, Geosystems* **13**, Q09007.

Giletti, B. J. & Casserly, J. E. D. (1994). Strontium diffusion kinetics in plagioclase feldspars. *Geochimica et Cosmochimica Acta* **58**, 3785–3793.

Giletti, B. J. & Shanahan, T. M. (1997). Alkali diffusion in plagioclase feldspar. *Chemical Geology* **139**, 3–20.

Gurenko, A. A. & Chaussidon, M. (1995). Enriched and depleted primitive melts included in olivine from Icelandic tholeiites—origin by continuous melting of a single mantle column. *Geochimica et Cosmochimica Acta* **59**, 2905–2917.

Halliday, A. N., Lee, D. C., Tommasini, S., Davies, G. R., Paslick, C. R., Fitton, J. G. & James, D. E. (1995). Incompatible trace-elements in oib and morb and source enrichment in the sub-oceanic mantle. *Earth and Planetary Science Letters* **133**, 379–395.

Harpp, K. S. & White, W. M. (2001). Tracing a mantle plume: Isotopic and trace element variations of Galapagos seamounts. *Geochemistry, Geophysics, Geosystems* **2**, 1042.

Hart, S. R. (1988). Heterogeneous mantle domains—signatures, genesis and mixing chronologies. *Earth and Planetary Science Letters* **90**, 273–296.

Hart, S. R. (1993). Equilibration during mantle melting—A fractal tree model. *Proceedings of the National Academy of Sciences of the USA* **90**, 11914–11918.

Hart, S. R., Hauri, E. H., Oschmann, L. A. & Whitehead, J. A. (1992). Mantle plumes and entrainment—isotopic evidence. *Science* **256**, 517–520.

Hart, S. R., Blusztajn, J., Dick, H. J. B., Meyer, P. S. & Muehlenbachs, K. (1999). The fingerprint of seawater circulation in a 500-meter section of ocean crust gabbros. *Geochimica et Cosmochimica Acta* **63**, 4059–4080.

Hauri, E. H., Whitehead, J. A. & Hart, S. R. (1994). Fluid dynamic and geochemical aspects of entrainment in mantle plumes. *Journal of Geophysical Research—Solid Earth* **99**, 24275–24300.

Hofmann, A. W. (1988). Chemical differentiation of the earth - the relationship between mantle, Continental-Crust, and Oceanic-Crust. *Earth and Planetary Science Letters* **90**, 297–314.

Hofmann, A. W. & Jochum, K. P. (1996). Source characteristics derived from very incompatible trace elements in Mauna Loa and Mauna Kea basalts, Hawaii Scientific Drilling Project. *Journal of Geophysical Research—Solid Earth* **101**, 11831–11839.

Huang, S. C., Frey, F. A., Blichert-Toft, J., Fodor, R. V., Bauer, G. R. & Xu, G. P. (2005). Enriched components in the Hawaiian plume: Evidence from Kahoolawe Volcano, Hawaii. *Geochemistry, Geophysics, Geosystems* **6**, Q11006.

Jaupart, C. & Tait, S. (1995). Dynamics of differentiation in magma reservoirs. *Journal of Geophysical Research—Solid Earth* **100**, 17615–17636.

Kamenetsky, V. S., Eggins, S. M., Crawford, A. J., Green, D. H., Gasparon, M. & Falloon, T. J. (1998). Calcic melt inclusions in primitive olivine at 43°N MAR: evidence for melt–rock reaction/melting involving clinopyroxene-rich lithologies during MORB generation. *Earth and Planetary Science Letters* **160**, 115–132.

Kelemen, P. B., Whitehead, J. A., Aharonov, E. & Jordahl, K. A. (1995). Experiments on flow focusing in soluble porous-media, with applications to melt extraction from the mantle. *Journal of Geophysical Research—Solid Earth* **100**, 475–496.

Kelley, K. A., Plank, T., Farr, L., Ludden, J. & Staudigel, H. (2005). Subduction cycling of U, Th, and Pb. *Earth and Planetary Science Letters* **234**, 369–383.

Kent, A. J. R., Baker, J. A. & Wiedenbeck, M. (2002). Contamination and melt aggregation processes in continental flood basalts: constraints from melt inclusions in Oligocene basalts from Yemen. *Earth and Planetary Science Letters* **202**, 577–594.

Kobayashi, K., Tanaka, R., Moriguti, T., Shimizu, K. & Nakamura, E. (2004). Lithium, boron, and lead isotope systematics of glass inclusions in olivines from Hawaiian lavas: evidence for recycled components in the Hawaiian plume. *Chemical Geology* **212**, 143–161.

Koleszar, A. M., Saal, A. E., Hauri, E. H., Nagle, A. N., Liang, Y. & Kurz, M. D. (2009). The volatile contents of the Galapagos plume; evidence for H_2O and F open system behavior in melt inclusions. *Earth and Planetary Science Letters* **287**, 442–452.

Kurz, M. D. & Geist, D. (1999). Dynamics of the Galapagos hotspot from helium isotope geochemistry. *Geochimica et Cosmochimica Acta* **63**, 4139–4156.

Kurz, M. D., Curtice, J., Fornari, D., Geist, D. & Moreira, M. (2009). Primitive neon from the center of the Galapagos hotspot. *Earth and Planetary Science Letters* **286**, 23–34.

Liang, Y. (2003). Kinetics of crystal–melt reaction in partially molten silicates: 1. Grain scale processes. *Geochemistry, Geophysics, Geosystems* **4**, 1045.

Maclennan, J. (2008). Lead isotope variability in olivine-hosted melt inclusions from Iceland. *Geochimica et Cosmochimica Acta* **72**, 4159–4176.

McDonough, W. F. & Sun, S. S. (1995). The composition of the Earth. *Chemical Geology* **120**, 223–253.

McKenzie, D., Stracke, A., Blichert-Toft, J., Albarède, F., Gronvold, K. & O'Nions, R. K. (2004). Source enrichment processes responsible for isotopic anomalies in oceanic island basalts. *Geochimica et Cosmochimica Acta* **68**, 2699–2724.

Porter, K. A. & White, W. M. (2009). Deep mantle subduction flux. *Geochemistry, Geophysics, Geosystems* **10**, Q12016.

Ren, Z. Y., Ingle, S., Takahashi, E., Hirano, N. & Hirata, T. (2005). The chemical structure of the Hawaiian mantle plume. *Nature* **436**, 837–840.

Reynolds, R. W. & Geist, D. J. (1995). Petrology of lavas from Sierra Negra volcano, Isabela Island, Galapagos archipelago. *Journal of Geophysical Research* **100**, 24537–24553.

Saal, A. E. & Van Orman, J. A. (2004). The Ra-226 enrichment in oceanic basalts: Evidence for melt–cumulate diffusive interaction processes within the oceanic lithosphere. *Geochemistry, Geophysics, Geosystems* **5**, Q02008.

Saal, A. E., Hart, S. R., Shimizu, N., Hauri, E. H., Layne, G. D. & Eiler, J. M. (2005). Pb isotopic variability in melt inclusions from the EMI–EMII–HIMU mantle end-members and the role of the oceanic lithosphere. *Earth and Planetary Science Letters* **240**, 605–620.

Saal, A. E., Kurz, M. D., Hart, S. R., Blusztajn, J. S., Blichert-Toft, J., Liang, Y. & Geist, D. J. (2007). The role of lithospheric gabbros on the composition of Galapagos lavas. *Earth and Planetary Science Letters* **257**, 391–406.

Schilling, J. G., Hanan, B. B., McCully, B., Kingsley, R. H. & Fontignie, D. (1994). Influence of the Sierra Leone mantle mlume on the Equatorial Mid-Atlantic Ridge—a Nd–Sr–Pb isotopic study. *Journal of Geophysical Research—Solid Earth* **99**, 12005–12028.

Sobolev, A. V. (1996). Melt inclusions in minerals as a source of principle petrological information. *Petrology* **4**, 209–220.

Sobolev, S. V. & Babeyko, A. Y. (1994). Modeling of mineralogical composition, density and elastic-wave velocities in anhydrous magmatic rocks. *Surveys in Geophysics* **15**, 515–544.

Sobolev, A. V., Hofmann, A. W. & Nikogosian, I. K. (2000). Recycled oceanic crust observed in 'ghost plagioclase' within the source of Mauna Loa lavas. *Nature* **404**, 986–990.

Sobolev, A. V., Hofmann, A. W., Jochum, K. P., Kuzmin, D. V. & Stoll, B. (2011). A young source for the Hawaiian plume. *Nature* **476**, 434–483.

Stracke, A., Hofmann, A. W. & Hart, S. R. (2005). FOZO, HIMU, and the rest of the mantle zoo. *Geochemistry, Geophysics, Geosystems* **6**, Q05007.

Vicenzi, E. P., McBirney, A. R., White, W. M. & Hamilton, M. (1990). The geology and geochemistry of Isla Marchena, Galapagos Archipelago: An ocean island adjacent to a mid-ocean ridge. *Journal of Volcanology and Geothermal Research* **40**, 291–315.

White, W. M., McBirney, A. R. & Duncan, R. A. (1993). Petrology and geochemistry of the Galapagos Islands—portrait of a pathological mantle plume. *Journal of Geophysical Research—Solid Earth* **98**, 19533–19563.

Workman, R. K. & Hart, S. R. (2005). Major and trace element composition of the depleted MORB mantle (DMM). *Earth and Planetary Science Letters* **231**, 53–72.

Workman, R. K., Hart, S. R., Jackson, M., Regelous, M., Farley, K. A., Blusztajn, J., Kurz, M. & Staudigel, H. (2004). Recycled metasomatized lithosphere as the origin of the enriched mantle II (EM2) end-member: Evidence from the Samoan volcanic chain. *Geochemistry, Geophysics, Geosystems* **5**, Q04008.

Yang, H. J., Frey, F. A., Weis, D., Giret, A., Pyle, D. & Michon, G. (1998). Petrogenesis of the flood basalts forming the Northern Kerguelen Archipelago: Implications for the Kerguelen plume. *Journal of Petrology* **39**, 711–748.

Yaxley, G. M. & Green, D. H. (1998). Reactions between eclogite and peridotite: Mantle refertilisation by subduction of oceanic crust. *Schweizerische Mineralogische und Petrographische Mitteilungen* **78**, 243–255.

Zimmer, M., Kroner, A., Jochum, K. P., Reischmann, T. & Todt, W. (1995). The Gabal-Gerf Complex—a Precambrian N-MORB ophiolite in the Nubian Shield, NE Africa. *Chemical Geology* **123**, 29–51.